"Matthew Effect": General Design Strategy of Fluorogenic Bioorthogonal Nanoprobes with Ultrahigh Emission Enhancement

Shinsuke Segawa[1], Xinwen OU[1], Tianruo Shen[2], Tomohiro Ryu[3], Yuki Ishii[3], Herman Sung[1], Ian Williams[1], Ryan T. K. Kwok[1], Kiyoshi Miyata[3], Ken Onda[3], Xuewen He[4], Xiaogang Liu[2], and Ben Tang[5]

[1]The Hong Kong University of Science and Technology
[2]Singapore University of Technology and Design
[3]Kyushu University
[4]Soochow University College of Chemistry Chemical Engineering and Materials Science
[5]The Chinese University of Hong Kong - Shenzhen

November 11, 2023

Abstract

Fluorescence imaging, a key technique in life science research, frequently utilizes fluorogenic probes for precise imaging in living systems. Tetrazine is an effective emission quencher in the design of fluorogenic probes, which can be selectively damaged upon bioorthogonal click reactions, leading to considerable emission enhancement. Despite significant efforts to increase the emission enhancement ratio upon click reaction (I_{AC}/I_{BC}) of tetrazine-functionalized fluorogenic probes, the influence of molecular aggregation on the emission properties has been largely overlooked in the design of these probes. In this study, we reveal that an ultrahigh I_{AC}/I_{BC} can be realized in the aggregate system when tetrazine is paired with aggregation-induced emission (AIE) luminogens. Tetrazine can increase its quenching efficiency upon aggregation and drastically reduce background emissions. Subsequent click reactions damage tetrazine and trigger significant AIE, leading to considerably enhanced I_{AC}/I_{BC}. We further showcase the capability of these ultra-fluorogenic systems in selective imaging of multiple organelles in living cells. We propose the term "Matthew Effect" in Aggregate Emission to describe the unique fluorogenicity of these probes, potentially providing a universal approach to attain ultrahigh emission enhancements in diverse fluorogenic aggregate systems.

1. Introduction

In recent decades, fluorescence imaging has emerged as a pivotal technique in life science for the direct visualization of dynamic living processes. Given the crowded nature of biological environments, achieving high-resolution imaging with an ultrahigh signal-to-noise ratio is of utmost importance for accurately monitoring chemical events. Therefore, significant efforts have been devoted to developing practical methodologies to obtain bright and high-resolution images. These strategies span from innovations in microscope design[1–6] and imaging system optimization[7] to intricate molecular-level[8–10] and nano-interface[11] engineering of fluorescent probes.

Fluorogenic probes, which refer to probes that can stimulate their emissions upon target recognition, represent a significant advancement in the pursuit of site-specific imaging with minimal background signals.[12,13] This milestone has been accomplished through the application of fluorescence quenching pathways.[14] For example, by linking an emission quencher to a fluorophore, the resulting fluorophore-quencher complex exhibits negligible emission. When the quencher is removed in response to specific biological events, the fluorophore's emission is restored, resulting in turn-on emission.[15] This characteristic defines the fluorophore-quencher

complex as a fluorogenic probe. To enhance contrast and achieve site-specific signals with these fluorogenic probes, the identification of easily removable and highly effective emission quenchers is essential.

Tetrazine, a benzene-like molecule with four embedded nitrogen atoms, has been identified as an ideal moiety to possess the aforementioned tunable fluorescence quenching properties. The quenched emission can be fully recovered after the tetrazine quencher is controllably decomposed upon photoirradiation[16] or through inverse electron demand Diels-Alder (iEDDA) reaction with strained alkene[17–19], alkyne[20], or isonitrile[21,22] groups. The iEDDA reaction has been successfully employed as a bioorthogonal click reaction that can selectively and instantly occur in the molecularly crowded environment inside biological systems.[23]Consequently, tetrazine-based fluorogenic dyes have been extensively developed, with significant efforts aiming at enhancing their emission enhancement ratio (I_{AC}/I_{BC}, whereI_{AC} and I_{BC} are the photoluminescence intensities after and before click reactions) by increasing tetrazine quenching efficiency. For example, initial studies started in the last decade focused on Förster Resonance Energy Transfer (FRET)[24,25] or through-bond energy transfer (TBET)[26,27] to direct n-π* emission quenching and ultrahigh I_{AC}/I_{BC}(>1000-fold) was achieved in blue to green probes via connecting fluorophore and tetrazine in proximity distance.[26] Later on, red to near-infrared turn-on emissions, which are challenging to attain through FRET or TBET-type quenching,[28] were realized by employing Dexter energy transfer (DET),[29]internal conversion (IC),[30–33] and photo-induced electron transfer (PeT) directed by sophisticated control of molecular conformations.[34] As a unique approach, molecular disaggregation upon iEDDA reaction was also applied to enhance the I_{AC}/I_{BC} of near-infrared (NIR) cyanine dyes.[35] These tetrazine-based fluorogenic dyes have been successfully employed in bioorthogonal imaging of various cellular targets such as lipids,[36] sugars,[37]proteins,[38] and nucleic acids.[39] However, most previous molecules were developed as single molecular systems, neglecting the concentration quenching or aggregation-caused quenching (ACQ) effect in living cell systems: conventional hydrophobic fluorophores with large π-conjugated structures inherently assemble in aqueous solutions, turning off their emission and resulting in weak turn-on signals as fluorogenic probes.[40,41] Indeed, in many cases,I_{AC}/I_{BC} measurements were conducted in organic solvents where molecular aggregation can be prevented.[16,33,42–48] To achieve ultrahighI_{AC}/I_{BC} in conditions that resemble cellular systems, it is desirable to develop fluorogenic systems in aggregate states.

Aggregation-induced emission luminogens (AIEgens) comprise a series of fluorescent dyes that exhibit weak emission in dilute solutions but can significantly enhance emission upon molecular aggregation.[49,50] Unlike conventional fluorophores that suffer from ACQ effects, AIEgens can achieve strong emissions even in aggregate states. Yet, there exist limited studies presenting tetrazine fluorogenic probes that exhibit aggregation-induced emission (AIE) properties post-iEDDA reaction.[51–53] One study reported a highI_{AC}/I_{BC} of up to 1779-fold, however it did not explicitly address the mechanism and relation between AIE properties and the highI_{AC}/I_{BC}.[51]Furthermore, the generalizability of such molecular design strategies remains unclear.

In this study, we demonstrated that by linking tetrazine to various AIEgens, the weakly-emissive tetrazine-AIEgen complex further suppresses their emission upon aggregation. Following an iEDDA reaction, the resulting emissive pyridazine compounds enhance their emission upon aggregation, affording ultrahighI_{AC}/I_{BC}. Further investigation concludes that this effect arises from the synergistic interplay between the intermolecular quenching effect of the tetrazine moiety and the AIE property of fluorogens. We also showcased that this ultra-fluorogenic system can be applied for site-selective fluorogenic imaging of multiple organelles in living cells, highlighting its potential for advanced imaging applications in biological systems. Drawing inspiration from the sociological term "Matthew Effect"[54] – describing the phenomenon that the rich become richer, and the poor become poorer – we coined this unique fluorogenisity as the "Matthew Effect" in Aggregate Emission, highlighting intensified darkness of quenched species and amplified brightness of emissive species in aggregate states. This "Matthew Effect" in Aggregate Emission potentially offers a universal strategy for achieving ultrahighI_{AC}/I_{BC} in fluorogenic nanoaggregate systems.

2. Results and Discussion

2.1. Initial design and synthesis

To investigate how nano-aggregation and AIEgens will affect the turn-on emission of tetrazine probes, we designed and synthesized a series of tetrazine-dye conjugates. Tetrazine units were synthesized under Pinner synthesis using thiol as a catalyst,[55] and sequential Pd-catalyzed coupling reactions connected tetrazine to chromophores. The obtained compounds were recrystallized whenever it was possible, and purity was confirmed by high-performance liquid chromatography (HPLC) to avoid impurity effects (shown in Figure S81-S90, Supporting Information). Their molecular structures were thoroughly characterized by nuclear magnetic resonance (NMR) spectroscopy and high-resolution mass spectra (shown in Figures S25-S56, Supporting Information). Single crystals were obtained except for MTPA-Tz, and X-ray diffraction analysis supports the structure[56] (Figures S20-S23, in Supporting Information). We prepared four AIEgen-tetrazine conjugates (AIE-Tz) and one normal planar fluorophore: pyrene-tetrazine conjugate (PR-Tz) as a negative control for the entire experiment. To obtain a multifaceted and general perspective of this strategy, we designed AIEgens with diverse structures that include either tetraphenyl ethylene (TPE-Tz) or triaryl amines (TPA-Tz, MTPA-Tz, and MBTPA-Tz) as well-known twisted units to achieve AIE properties. As expected, all molecules reacted quantitatively with the strained alkyne compound (1R,8S,9s)-Bicyclo[6.1.0]non-4-yn-9-ylmethanol (BCN-OH) to provide emissive pyridazine compounds (Figure 1A), and the obtained AIE-Pzs covered a broad emission range from violet to NIR (380 to 780 nm) in water (Figure 1B) with an emission maximum at 419 nm, 481 nm, 538 nm, 636 nm for TPA-Pz, TPE-Pz, MTPA-Pz, and MBTPA-Pz, respectively.

2.2. Photoluminescence measurements of AIE-Tz

After synthesizing AIE-Tz, we investigated their emission properties in dilute solutions in DMSO and aggregates in water. Not surprisingly, both AIE-Tzs and PR-Tz only exhibited very weak emissions in dilute solutions (quantum yield < 0.002, shown in Table S1, Supporting Information). This could be due to two reasons: firstly, AIEgens do not show strong emission in solution because of their molecular motions,[57] and secondly, the tetrazine unit acts as a quenching unit. However, we still observed non-negligible emissions from AIEgens or pyrene moieties that could cause background emission problems during fluorescence imaging. By changing the water fraction, molecular aggregation was observed with dynamic laser scattering measurements (Figure S5, Supporting Information). Interestingly, not only does PR-Tz, whose fluorophore is impacted by the aggregation-caused quenching effect, show further quenched emission upon molecular aggregation, but also AIE-Tzs, which are expected to exhibit enhanced emission, demonstrate further suppressed emission under the same conditions (Figure 2D), apart from the negligible emissions from the tetrazine moiety peaked at around 600 nm (Figure S2, Supporting Information). Specifically, TPE-Tz exhibited very weak emission at 470 nm coming from tetraphenyl ethylene core[58], and this emission's intensity decreased upon aggregation (Figure 2A). TPA-based tetrazine molecules displayed slightly stronger emission than TPE-Tz in dilute solution, and the emission was well quenched upon water addition (Figure 2B). This more notable emission of TPA tetrazine adducts over TPE-Tz could be a consequence of the less flexible structure of TPA units compared to TPE units. Indeed, PR-Tz, which has the most rigid structure, showed the strongest emission among all tetrazine compounds in DMSO, and a significant emission decrease was observed upon water addition (Figure 2C). This phenomenon of AIE-Tz suppressing its emission upon aggregation effectively highlights tetrazine's potential to reduce the background signals from fluorogenic dyes, thereby contributing to ultrahigh fluorescence turn-on ratios in the aggregate state. This intriguing observation further spurred our interest to explore this quenching effect more thoroughly.

2.3. Intermolecular quenching effect of AIE-Tz.

To understand why AIE-Tz exhibits emission quenching in the aggregate state despite the incorporation of AIEgens, we further investigated the interaction between the tetrazine moiety and AIEgens in the aggregate state. Single crystal X-ray diffraction (XRD) analysis and molecular dynamics (MD) simulations were conducted to obtain aggregate models of MBTPA-Tz, and intermolecular center-to-center distances between the tetrazine and surrounding aryl rings were calculated. As expected, we observed proximal molecular interactions in the aggregate state: 3.6-4.7 Å from the XRD result and 3.9-4.9 Å from the MD calculation (Figure S6-10, S24 in Supporting Information). The single crystal structure of MBTPA-Tz reveals a

tetrazine-chromophore distance as close as 3.668 Å (Figure 3A). This distance is comparable to or even shorter than that of reported tetrazine fluorogenic dyes known to efficiently quench emissions through energy transfer mechanisms.[29] Therefore, this result indicates that tetrazine can enhance emission quenching efficiency upon aggregation via intermolecular interactions with AIEgens. This intermolecular quenching effect of the tetrazine unit was experimentally confirmed using a commercially available AIEgen (TPE-CN) as a fluorescence indicator (Figure 3B). We measured the emission intensity of 10 μM TPE-CN, co-aggregated with TPE-Tz at different concentrations. Consequently, we observed that the emission of the aggregate was apparently quenched by 50.3% with 0.1 μM TPE-Tz addition; the emission intensity dropped 94.6% and even 99.7% with 1 μM and 10 μM TPE-Tz addition, respectively (Figure 3B). Considering there is no direct through-bond connection between TPE-CN and TPE-Tz, this quenching effect arises from intermolecular interactions between TPE-Tz and TPE-CN directed by aggregation.

2.4. Photoluminescence measurements of AIE-Pz

Tetrazine quenchers were easily converted to pyridazine moieties by BCN-OH addition, and the aggregate emission of the obtained AIE-Pz was next investigated. Similar to AIE-Tz, AIE-Pz forms aggregates upon increasing water fraction. Because the tetrazine quencher is removed, AIE-Pz exhibits stronger emission both in dilute solutions and aggregates (Table S1, Supporting Information). Most importantly, AIE-Pzs demonstrates enhanced emission upon aggregation, unlike AIE-Tzs (Figure 4D). Specifically, TPE-Pz and MBTPA-Pz display the most typical AIE properties (Figure 4A), with significantly increased emission upon water addition. In contrast, TPA-Pz and MTPA-Pz exhibit twisted-intramolecular charge transfer (TICT)[59] type AIEgen-like behavior: upon water addition, increased polarity causes charge separation in the excited state, initially quenching the emission. However, as the water fraction further increases, the emission is turned on again, induced by aggregate formation (Figure 4B). The PR-Pz negative control suffers from the ACQ effect and quenches its emission upon aggregation as expected (Figure 4C). In short, we achieved an emission enhancement system in AIE-Pzs aggregates.

2.5. Turn-on emissions of AIE-Tz upon "click" reaction

We successfully achieved a unique system in which non-emissive tetrazine molecules become even darker, and emissive pyridazine molecules become even brighter in aggregate states. Encouraged by this result, we calculated the emission enhancement ratio upon click reaction (I_{AC}/I_{BC}) in the aggregate state to verify the impact of this aggregation-formation strategy on the emission enhancement ratio. The PR-Tz negative control demonstrated a very weak I_{AC}/I_{BC} around 20 in an aqueous environment due to the strong ACQ effect in water (Figure 5B) In contrast, TPE-Tz, possessing the most canonical AIEgen unit, displayed a significantly high emission enhancement ratio ofI_{AC}/I_{BC} up to 4833 (Figure 5A, C). Even TPA derivatives, which act as less active AIE units, resulted in a high emission enhancement ratio upon click reaction (Figure S4, Supporting Information), as evidenced by MTPA-Tz (I_{AC}/I_{BC} = 2439) and MBTPA-Tz (I_{AC}/I_{BC} = 209). Only TPA-Tz did not exhibit strong turn-on emission (I_{AC}/I_{BC} = 93) among AIE-Tz, as the post-click reaction compound was still affected by n-π* type quenching from the pyridazine group and did not exhibit a strong emission (quantum yield < 0.02, Table S1 and Figure S16 in Supporting Information).

Multiple reports suggest a negative correlation between emission wavelengths[25,28,60] and emission enhancement ratios for tetrazine fluorogenic probes. To confirm this, we plottedI_{AC}/I_{BC} values of previously reported tetrazine dyes against their emission wavelength. As a result, the plotted data points revealed a distinct and consistent trend, illustrating that as the emission wavelength increased, the emission enhancement ratio decreased. This visualization successfully substantiated the negative correlation between these two parameters. Most importantly, we observed that AIE-Tz demonstrated a very strong turn-on property compared to previously reported molecules in each emission wavelength. Notably, the 4833-fold emission enhancement of TPE-Tz is one of the best values among previous reports (Figure 5C and Table S2, Supporting Information). In conclusion, we discovered that connecting AIEgens to tetrazine units is an effective and general strategy for achieving strong fluorogenic signals in aqueous systems that inevitably cause aggregation of hydrophobic molecules.

2.6. Theoretical investigation of tetrazine quenching mechanism

To better understand the quenching mechanism and turn-on mechanism, density functional theory (DFT) and time-dependent DFT (TD-DFT) calculations were carried out on MBTPA-Tz and its post-iEDDA reaction compound MBTPA-Pz in single molecule and aggregate states. We focused on these molecules considering MBTPA-Pz's long emission wavelength and high$I_{\mathrm{AC}}/I_{\mathrm{BC}}$, which is ideal for biological applications. A comprehensive explanation of the assignment process for individual excited states can be found in section 3 of Supporting Information.

Tetrazine moieties cause significant emission quenching through various mechanisms. In general, the primary quenching mechanism involves accessing the dark n-π* transition state in the tetrazine moiety. When the tetrazine moiety is conjugated with a chromophore, this access comes from the internal conversion process, termed internal conversion to dark state (ICDS).[31] Alternatively, when access comes from energy transfer processes such as FRET[60] or DET[29] between tetrazine and fluorophore, the quenching process is summarized as energy transfer to dark state (ETDS).[25] Additionally, when tetrazine is located close to a fluorophore, the electron-deficient tetrazine unit can act as a strong acceptor, causing a non-radiative electron-transferred (ET) state through the PeT mechanism.[34] At the same time, AIEgens with highly twisted and rotational structures are well known to quench their emission through molecular motion.[57] As one of the molecular flexibility triggering quenching states, we focused on the twisted-intramolecular charge transfer (TICT)[59,61] state, in which molecules are twisted to intramolecularly separate charge between electron-rich and electron-poor moieties that cause weaker emission.

When we investigate our system (Figure 6), not surprisingly, we observed two major non-radiative states under the emissive π-π* state in MBTPA-Tz molecular state: 1) the dark n-π* state caused by the tetrazine unit and 2) the TICT state caused by the AIEgen. Those states were confirmed as dark states by their negligible oscillator strength values ($f < 0.01$). For MBTPA-Tz, tetrazine is conjugated with AIEgen; therefore, the access to the dark n-π* state is from internal conversion. We determined that emission quenching is due to both ICDS and TICT processes. Once MBTPA-Tz is aggregated, the dark state characteristics change. Restricted molecular configuration prohibits access to the TICT quenching state. Instead, we found a newly formed dark ET state whose hole and electron are separated in two molecules, accompanied by low-lying dark n-π* states induced by the tetrazine moieties.

This result matches the intermolecular quenching effect observed in AIE-Tz molecules: close interaction between tetrazine and AIEgen induces PeT quenching and provides intermolecular access to the n-π* dark state through energy transfer as well as maintaining internal conversion pathways. In summary, MBTPA-Tz aggregate quenches emission based on ICDS, ETDS, and PeT processes. These multiple quenching pathways amplify the quenching effect of tetrazine and explain the experimental result of the aggregation-enhanced quenching effect of MBTPA-Tz (Figure 2).

Upon iEDDA reaction, the tetrazine moiety is damaged, and the tetrazine-triggered quenching states are henceforward eliminated. As a result, the pyridazine molecule exhibits different behavior. In the single-molecule state of MBTPA-Pz, the n-π* dark state is no longer observed, but the twisted-intramolecular charge transfer (TICT) state persists, resulting in weak fluorescence in dilute solution. However, when aggregation occurs, the TICT formation is restricted due to the limited free volume and hydrophobic environment in the solid state. Consequently, no quenching state exists beneath the emissive π-π* state, allowing for strong emission in the MBTPA-Pz aggregate. As a result, the emission of MBTPA-Pz is switched on as access to the TICT dark state is inhibited in the aggregate state.

2.7. "Matthew Effect" in Aggregate Emission

In short, we successfully developed a system in which non-emissive tetrazine-containing molecules become even less emissive, and emissive pyridazine molecules become even more emissive in the aggregate state, resulting in ultra-high emission enhancement ratios. We refer to this effect as the "Matthew Effect" in Aggregate Emission (Figure 7), drawing from the sociological term that describes the phenomenon in which the poor become poorer, and the rich become richer in academic society.[54] Given that the intermolecular

quenching effect is not limited to the tetrazine moiety, we anticipate additional "Matthew Effect" in Aggregate Emission reports in the future, which can be designed by connecting AIEgens to emission quencher.

2.8. Bioorthogonal fluorogenic live cell imaging

Lastly, we applied the fluorogenic nanoaggregate for bioorthogonal fluorogenic imaging in living cells. First, MBTPA-Tz was added to cells, and confocal laser microscopy was used to observe the emission signals inside the cells. As expected, no emission was observed even after a 60 min incubation (Figure 8B). After washing the cells thoroughly, BCN-OH was added and incubated for 30 min, resulting in the observation of turn-on emission inside the cell without the washing procedure (Figure S18, Supporting Information). This result confirms that the iEDDA reaction between MBTPA-Tz and BCN-OH can bioorthogonaly take place in congested living systems.

To utilize this bioorthogonal turn-on emission for more specific purposes, the hydroxy group of BCN-OH was functionalized with several side chains targeting specific organelles: a triphenylphosphine group (TPP) to target mitochondria, a 1,2-dipalmitoyl-sn-glycero-3-phosphoethanolamine (DPPE) unit to target the cell membrane, and a halotag ligand (Halo) to localize to the hydrophobic environment inside the cell. These compounds were designated as BCNTPP, BCNDPPE, and BCNHalo, correspondingly (Figure 8A). The biocompatibility of MBTPA-Tz and these BCN compounds were confirmed by MTT assay (Figure S17). By adding BCNTPP or BCNHalo to cells incubated with MBTPA-Tz, strong turn-on emission was observed at the mitochondria and lipid droplets, respectively. Here, excellent colocalization signals alongside commercially available organelle-staining dyes (MitoTracker Deep Red FM and BODIPY 493/503) were observed, with Pearson correlation coefficients up to 0.95 and 0.84 (Figure 8C, E), respectively. However, when BCNDPPE was added, no turn-on emission was observed at the cell membrane. This could likely be attributed to BCNDPPE being initially internalized into the cell and taking some time to be expressed on the cell surface. To address this problem, BCNDPPE was added first and allowed to incubate for 24 hours, followed by a thorough washing of the cells and the subsequent addition of MBTPA-Tz. As a result, strong turn-on emission was observed at the cellular membrane (Figure 8D), which was further confirmed by colocalized signals using a commercially available membrane tracker (CellMask Plasma Membrane Stains) with a Pearson correlation coefficient of up to 0.93.

Consequently, MBTPA-Tz aggregates were proven to selectively target and visualize biological targets labeled with a strained alkyne group. To our best knowledge, this is the first example of tetrazine functionalized AIEgen for imaging multiple cellular environments. Previous reports only addressed to mitochondria imaging applications.[51–53] Therefore, this result highlights the flexible localization property of AIEgen-based nanoprobe, which expands the applications of this bioorthogonally activatable fluorogenic systems. Furthermore, it is noteworthy that it shows better photo-bleaching stability than any commercially available bioprobes used in this study (Figure S19, Supporting Information). These compelling findings provide substantial evidence that the MBTPA-Tz nanoprobe can effectively serve as a versatile biological imaging tool, as demonstrated by its exceptional multi-organelle targeting capabilities.

3. Conclusion

In this study, we have demonstrated a general strategy to develop ultra-highly fluorogenic tetrazine probes: By connecting a tetrazine quencher to an AIEgen, we observed a unique feature where non-emissive tetrazine compounds further quench their emission upon aggregation, and emissive pyridazine compounds enhance their emission upon aggregation. We termed this effect, which significantly enhances the emission enhancement ratio, as the "Matthew Effect" in Aggregate Emission.

Based on the experimental and theoretical investigation, we concluded that this "Matthew Effect" in Aggregate Emission arises from the synergetic effects of intermolecular quenching of the tetrazine moiety and aggregation-induced emission properties induced by AIEgens.

Lastly, we demonstrated that this highly fluorogenic aggregate can be applied for bioorthogonal fluorogenic imaging in living cells: by controlling the BCN location, we can observe turn-on signals in specific cellular

environments such as mitochondria, cellular membranes, and lipid droplets. Considering recent advances in bioorthogonal chemistry to non-genetically label biological systems with clickable handles, this fluorogenic aggregate will become a key tool to visualize various molecular events inside living systems.

Based on its mechanism, the "Matthew Effect" in Aggregate Emission is expected to be realized not only by tetrazine but also by any emission quenchers when they are connected to an AIEgen. Therefore, this report will pave the way for a general strategy to achieve high turn-on emissions by transcending single molecular properties through aggregate formation.

Acknowledgements

We would like to express our deepest gratitude to Prof. Terence Wong at The Hong Kong University of Science and Technology, Prof. Motonari Uesugi at Kyoto University, Dr. Hiromichi V. Miyagishi at Hokkaido University, Prof. Neal K. Devaraj at the University of California, San Diego, and Prof. K. Barry Sharpless and Dr. John Cappiello at Scripps Research for their invaluable guidance, comments, and insightful suggestions. The authors acknowledge the funding support of Hong Kong PhD Fellowship Scheme (PF18-15484), the National Natural Science Foundation of China (21788102 and 22274106), the Research Grants Council of Hong Kong (16306620, 16303221, N_HKUST609/19, and C6014-20W), the Innovation and Technology Commission (ITC-CNERC14SC01), and Shenzhen Science and Technology Innovation Committee (JCYJ20180507183832744). This work was partly supported by JSPS KAKENHI (JP23H01977, JP23H04631), JST the establishment of university fellowships towards the creation of science technology innovation (JPMJFS2132).

Conflict of Interests

The authors declare no conflict of interests.

Data Availability Statement

The data that supports the findings of this study are available in the supplementary material of this article

Supporting Information

Supporting Information is available from the Wiley Online Library or from the author.

Received: ((will be filled in by the editorial staff)) Revised: ((will be filled in by the editorial staff)) Published online: ((will be filled in by the editorial staff))

References

[1] M. G. L. Gustafsson, *Proc. Natl. Acad. Sci. U. S. A.***2005** , *102* , 13081.

[2] E. Betzig, G. H. Patterson, R. Sougrat, O. W. Lindwasser, S. Olenych, J. S. Bonifacino, M. W. Davidson, J. Lippincott-Schwartz, H. F. Hess, *Science* **2006** , *313* , 1642.

[3] S. T. Hess, T. P. K. Girirajan, M. D. Mason, *Biophys. J.***2006** , *91* , 4258.

[4] M. J. Rust, M. Bates, X. Zhuang, *Nat. Methods***2006** , *3* , 793.

[5] S. W. Hell, J. Wichmann, *Opt. Lett.* **1994** ,*19* , 780.

[6] Z. Liu, L. D. Lavis, E. Betzig, *Mol. Cell* **2015** ,*58* , 644.

[7] A. Sharonov, R. M. Hochstrasser, *Proc. Natl. Acad. Sci. U. S. A.* **2006** , *103* , 18911.

[8] S.-N. Uno, M. Kamiya, T. Yoshihara, K. Sugawara, K. Okabe, M. C. Tarhan, H. Fujita, T. Funatsu, Y. Okada, S. Tobita, Y. Urano, *Nat. Chem.* **2014** , *6* , 681.

[9] J. Tyson, K. Hu, S. Zheng, P. Kidd, N. Dadina, L. Chu, D. Toomre, J. Bewersdorf, A. Schepartz, *ACS Cent Sci* **2021** ,*7* , 1419.

[10] Q. Zheng, A. X. Ayala, I. Chung, A. V. Weigel, A. Ranjan, N. Falco, J. B. Grimm, A. N. Tkachuk, C. Wu, J. Lippincott-Schwartz, R. H. Singer, L. D. Lavis, *ACS Cent Sci* **2019** , *5* , 1602.

[11] X. Yang, K. Zhanghao, H. Wang, Y. Liu, F. Wang, X. Zhang, K. Shi, J. Gao, D. Jin, P. Xi, *ACS Photonics* **2016** ,*3* , 1611.

[12] X. Li, X. Gao, W. Shi, H. Ma, *Chem. Rev.* **2014** ,*114* , 590.

[13] G. A. Lemieux, C. L. De Graffenried, C. R. Bertozzi, *J. Am. Chem. Soc.* **2003** , *125* , 4708.

[14] M. J. Hangauer, C. R. Bertozzi, *Angew. Chem. Int. Ed***2008** , *47* , 2394.

[15] S. Leng, Q.-L. Qiao, Y. Gao, L. Miao, W.-G. Deng, Z.-C. Xu,*Chin. Chem. Lett.* **2017** , *28* , 1911.

[16] A. Loredo, J. Tang, L. Wang, K.-L. Wu, Z. Peng, H. Xiao,*Chem. Sci.* **2020** , *11* , 4410.

[17] N. K. Devaraj, R. Weissleder, S. A. Hilderbrand,*Bioconjug. Chem.* **2008** , *19* , 2297.

[18] D. M. Patterson, L. A. Nazarova, B. Xie, D. N. Kamber, J. A. Prescher, *J. Am. Chem. Soc.* **2012** , *134* , 18638.

[19] M. L. Blackman, M. Royzen, J. M. Fox, *J. Am. Chem. Soc.***2008** , *130* , 13518.

[20] K. Lang, L. Davis, S. Wallace, M. Mahesh, D. J. Cox, M. L. Blackman, J. M. Fox, J. W. Chin, *J. Am. Chem. Soc.* **2012** ,*134* , 10317.

[21] J. Tu, D. Svatunek, S. Parvez, A. C. Liu, B. J. Levandowski, H. J. Eckvahl, R. T. Peterson, K. N. Houk, R. M. Franzini, *Angew. Chem. Int. Ed.* **2019** , *58* , 9043.

[22] M. Xu, T. Deb, J. Tu, R. M. Franzini, *J. Org. Chem.***2019** , *84* , 15520.

[23] C. P. Ramil, Q. Lin, *Chem. Commun.* **2013** ,*49* , 11007.

[24] N. K. Devaraj, S. Hilderbrand, R. Upadhyay, R. Mazitschek, R. Weissleder, *Angew. Chem. Int. Ed.* **2010** , *49* , 2869.

[25] W. Chi, L. Huang, C. Wang, D. Tan, Z. Xu, X. Liu, *Mater. Chem. Front* **2021** , *5* , 7012.

[26] L. G. Meimetis, J. C. T. Carlson, R. J. Giedt, R. H. Kohler, R. Weissleder, *Angew. Chem. Int. Ed.* **2014** , *53* , 7531.

[27] G. Knorr, E. Kozma, A. Herner, E. A. Lemke, P. Kele, *Chem Eur J* **2016** , *22* , 8972.

[28] L. Chen, F. Li, M. Nandi, L. Huang, Z. Chen, J. Wei, W. Chi, X. Liu, J. Yang, *Dyes Pigm.* **2020** , *177* , 108313.

[29] P. Werther, K. Yserentant, F. Braun, K. Grußmayer, V. Navikas, M. Yu, Z. Zhang, M. J. Ziegler, C. Mayer, A. J. Gralak, M. Busch, W. Chi, F. Rominger, A. Radenovic, X. Liu, E. A. Lemke, T. Buckup, D.-P. Herten, R. Wombacher, *ACS. Cent. Sci.* **2021** , *7* , 1561.

[30] Y. Lee, W. Cho, J. Sung, E. Kim, S. B. Park, *J. Am. Chem. Soc.* **2018** , *140* , 974.

[31] T. Shen, W. Zhang, P. Yadav, X. W. Sun, X. Liu, *Mater. Chem. Front.* **2023** , *7* , 1082.

[32] T. S.-M. Tang, H.-W. Liu, K. K.-W. Lo, *Chem. Commun.***2017** , *53* , 3299.

[33] W. Mao, J. Tang, L. Dai, X. He, J. Li, L. Cai, P. Liao, R. Jiang, J. Zhou, H. Wu, *Angew. Chem. Int. Ed.* **2021** ,*60* , 2393.

[34] W. Mao, W. Chi, X. He, C. Wang, X. Wang, H. Yang, X. Liu, H. Wu, *Angew. Chem. Int. Ed.* **2022** , *61* , e202117386.

[35] X. Zhang, J. Gao, Y. Tang, J. Yu, S. S. Liew, C. Qiao, Y. Cao, G. Liu, H. Fan, Y. Xia, J. Tian, K. Pu, Z. Wang, *Nat. Commun.***2022** , *13* , 3513.

[36] L. Chen, F. Li, Y. Li, J. Yang, Y. Li, B. He, *Chem. Commun.* **2021** , *58* , 298.

[37] S. Stairs, A. A. Neves, H. Stöckmann, Y. A. Wainman, H. Ireland-Zecchini, K. M. Brindle, F. J. Leeper, *Chembiochem***2013** , *14* , 1063.

[38] J. L. Seitchik, J. C. Peeler, M. T. Taylor, M. L. Blackman, T. W. Rhoads, R. B. Cooley, C. Refakis, J. M. Fox, R. A. Mehl, *J. Am. Chem. Soc.* **2012** , *134* , 2898.

[39] P. N. Asare-Okai, E. Agustin, D. Fabris, M. Royzen, *Chem. Commun.* **2014** , *50* , 7844.

[40] G. S. Beddard, S. E. Carlin, G. Porter, *Chem. Phys. Lett.* **1976** , *43* , 27.

[41] Y. Huang, J. Xing, Q. Gong, L.-C. Chen, G. Liu, C. Yao, Z. Wang, H.-L. Zhang, Z. Chen, Q. Zhang, *Nat. Commun.* **2019** ,*10* , 169.

[42] W. Shi, J. Li, X. He, S. Zhou, H. Sun, H. Wu, *Org. Lett.***2022** , *24* , 3368.

[43] P. E. Z. Klier, A. M. M. Gest, J. G. Martin, R. Roo, M. X. Navarro, L. Lesiak, P. E. Deal, N. Dadina, J. Tyson, A. Schepartz, E. W. Miller, *J. Am. Chem. Soc.* **2022** , *144* , 12138.

[44] M. E. Graziotto, L. D. Adair, A. Kaur, P. Vérité, S. R. Ball, M. Sunde, D. Jacquemin, E. J. New, *RSC Chem Biol* **2021** ,*2* , 1491.

[45] S. J. Siegl, J. Galeta, R. Dzijak, M. Dračínský, M. Vrabel,*Chempluschem* **2019** , *84* , 493.

[46] D. Wu, D. F. O'Shea, *Chem. Commun.* **2017** ,*53* , 10804.

[47] A. Yazdani, N. Janzen, S. Czorny, R. G. Ungard, T. Miladinovic, G. Singh, J. F. Valliant, *Dalton Trans.* **2017** , *46* , 14691.

[48] H. Wu, J. Yang, J. Šečkutė, N. K. Devaraj, *Angew. Chem. Int. Ed* **2014** , *53* , 5805.

[49] J. Luo, Z. Xie, J. W. Y. Lam, L. Cheng, H. Chen, C. Qiu, H. S. Kwok, X. Zhan, Y. Liu, D. Zhu, Others, *Chem. Commun.***2001** , 1740.

[50] Y. Hong, J. W. Y. Lam, B. Z. Tang, *Chem. Soc. Rev.***2011** , *40* , 5361.

[51] Y. Wang, Y. Teng, H. Yang, X. Li, D. Yin, Y. Tian, *Chem. Commun.* **2022** , *58* , 949.

[52] S.-K. Choi, Y. Lee, S. E. Yoon, H. Choi, J. Kim, J. H. Kim, S. Lee, W. Kim, E. Kim, *Sens. Actuators B Chem.* **2021** ,*340* , 129966.

[53] Y. Teng, R. Zhang, B. Yang, H. Yang, X. Li, D. Yin, X. Feng, Y. Tian, *J. Mater. Chem. B.* **2022** , *10* , 8642.

[54] R. K. Merton, *Science* **1968** , *159* , 56.

[55] W. Mao, W. Shi, J. Li, D. Su, X. Wang, L. Zhang, L. Pan, X. Wu, H. Wu, *Angew. Chem. Int. Ed.* **2019** , *58* , 1106.

[56] CCDC 2263531 (for PR-Tz), 2263532 (for MBTPA-Tz), 2263533 (for TPA-Tz), and 2263534 (for TPE-Tz) contain the supplementary crystallographic data for this paper. These data can be obtained free of charge from The Cambridge Crystallographic Data Centre via www.ccdc.cam.ac.uk/structurese.

[57] N. L. C. Leung, N. Xie, W. Yuan, Y. Liu, Q. Wu, Q. Peng, Q. Miao, J. W. Y. Lam, B. Z. Tang, *Chem. Eur. J.* **2014** ,*20* , 15349.

[58] L. Huang, H. Tao, S. Zhao, K. Yang, Q.-Y. Cao, M. Lan,*Ind. Eng. Chem. Res.* **2020** , *59* , 8252.

[59] S. Sasaki, G. P. C. Drummen, G.-I. Konishi, *J. Mater. Chem.* **2016** , *4* , 2731.

[60] B. Pinto-Pacheco, W. P. Carbery, S. Khan, D. B. Turner, D. Buccella, *Angew. Chem. Int. Ed* **2020** , *59* , 22140.

[61] K. Hanaoka, S. Iwaki, K. Yagi, T. Myochin, T. Ikeno, H. Ohno, E. Sasaki, T. Komatsu, T. Ueno, M. Uchigashima, T. Mikuni, K. Tainaka, S. Tahara, S. Takeuchi, T. Tahara, M. Uchiyama, T. Nagano, Y. Urano,*J. Am. Chem. Soc.* **2022** , *144* , 19778.

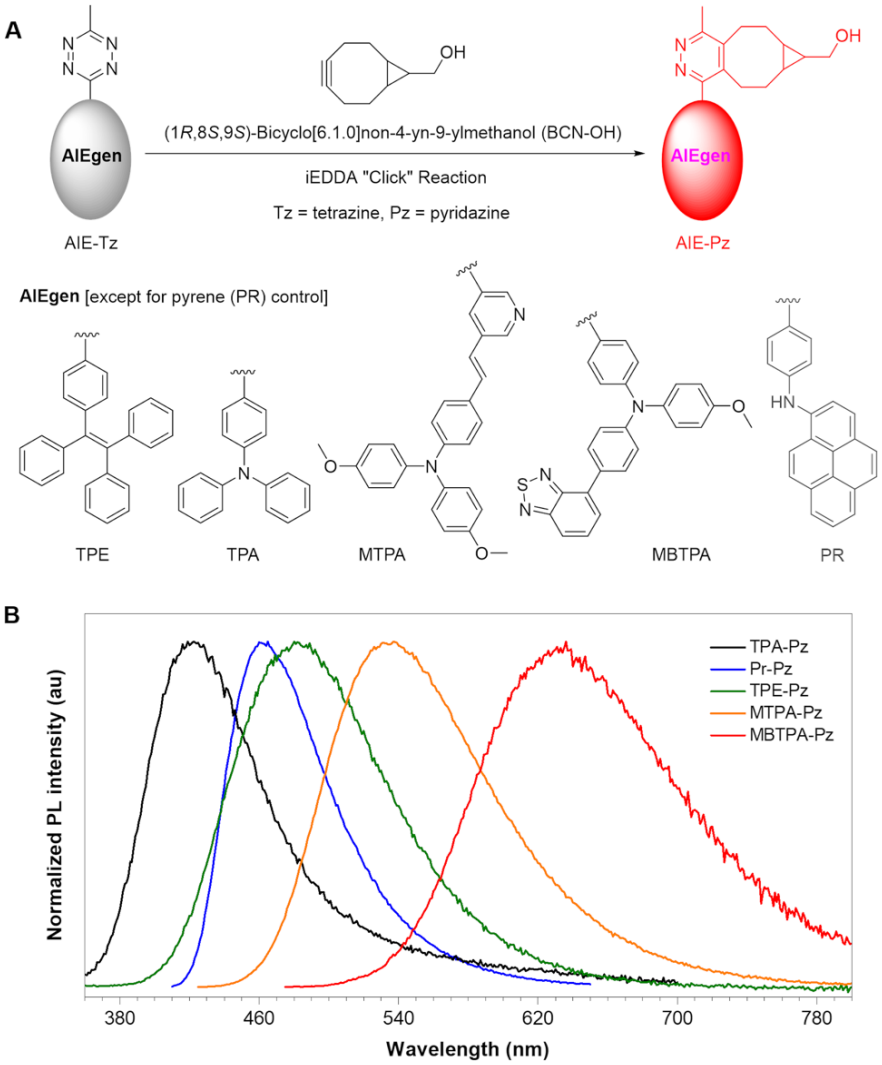

Figure 1. A) Design of fluorogenic probe using tetrazine (Tz) as an emission quencher and BCN-OH as a turn-on switch; AIE = aggregation-induced emission, AIEgen = AIE luminogen, iEDDA = inverse electron-demand Diels-Alder. B) Photoluminescence (PL) spectra of the fluorogens synthesized in this work.

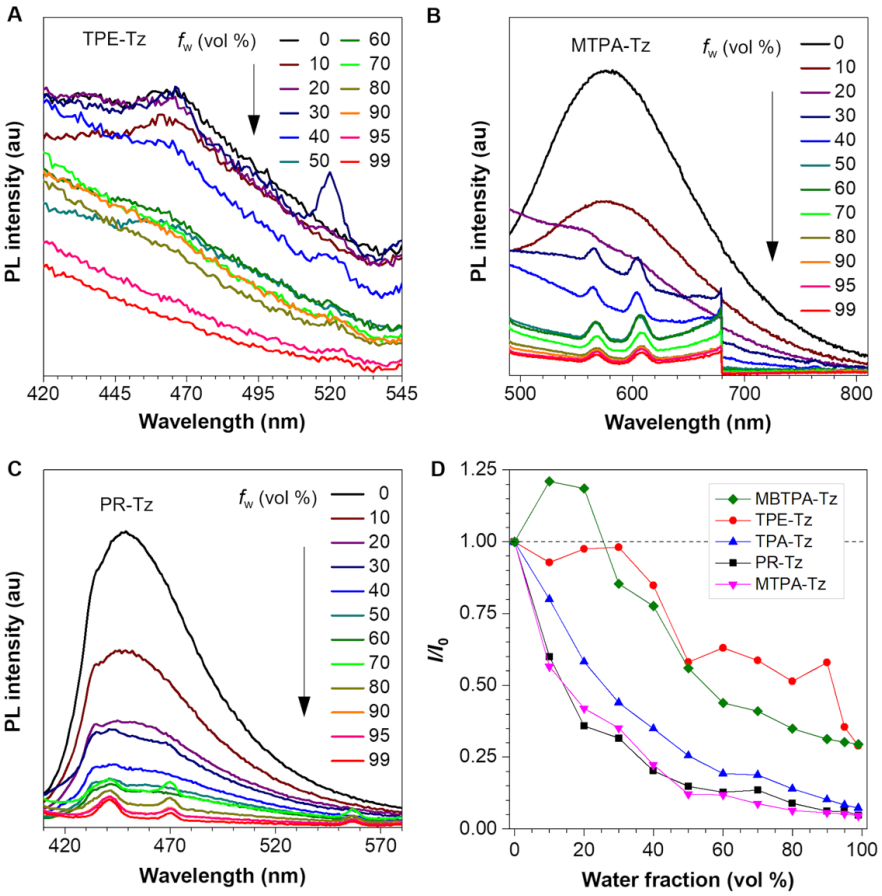

Figure 2. Aggregation-enhanced quenching of chromophore-tetrazine (Ch-Tz) adducts. PL spectra of (A) TPE-Tz, (B) MTPA-Tz, and (C) PR-Tz in the DMSO/water mixtures with different fractions of water (f_w). D) Plots of emission maxima of Ch-Tz adducts against water fractions in the aqueous mixtures. It needs to be noted that since the compounds are all dark tetrazine species, the emission intensities here are significantly low. Therefore, some inevitable noise was also captured to obtain these minimum signals with this magnified view. Nevertheless, most importantly, a clear trend of enhanced quenching upon aggregation was observed.

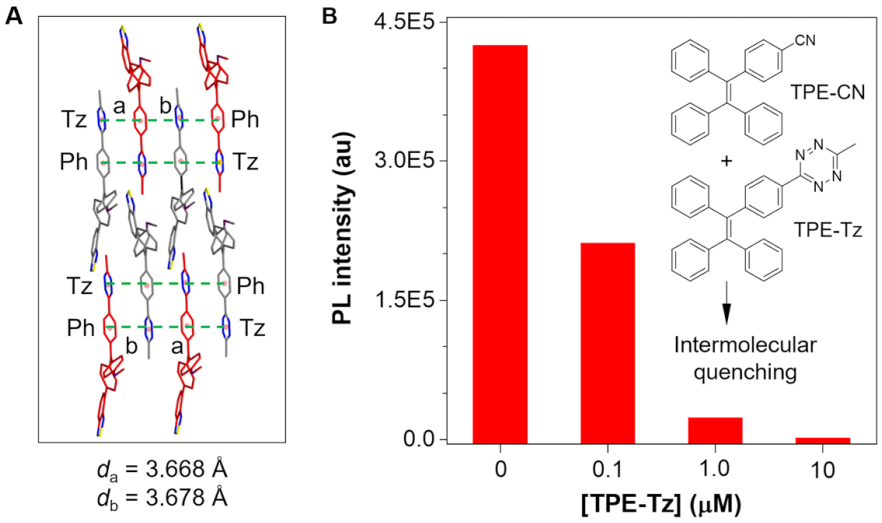

Figure 3. A) Intermolecular interaction between tetrazine (Tz; acceptor) and phenyl (Ph; donor) rings in the crystal structure of MBTPA-Tz. B) PL quenching of TPE-CN (10 μM) by the intermolecular interaction with TPE-Tz in their aggregates in the DMSO/water mixture (f_w = 99 vol %). d = distance.

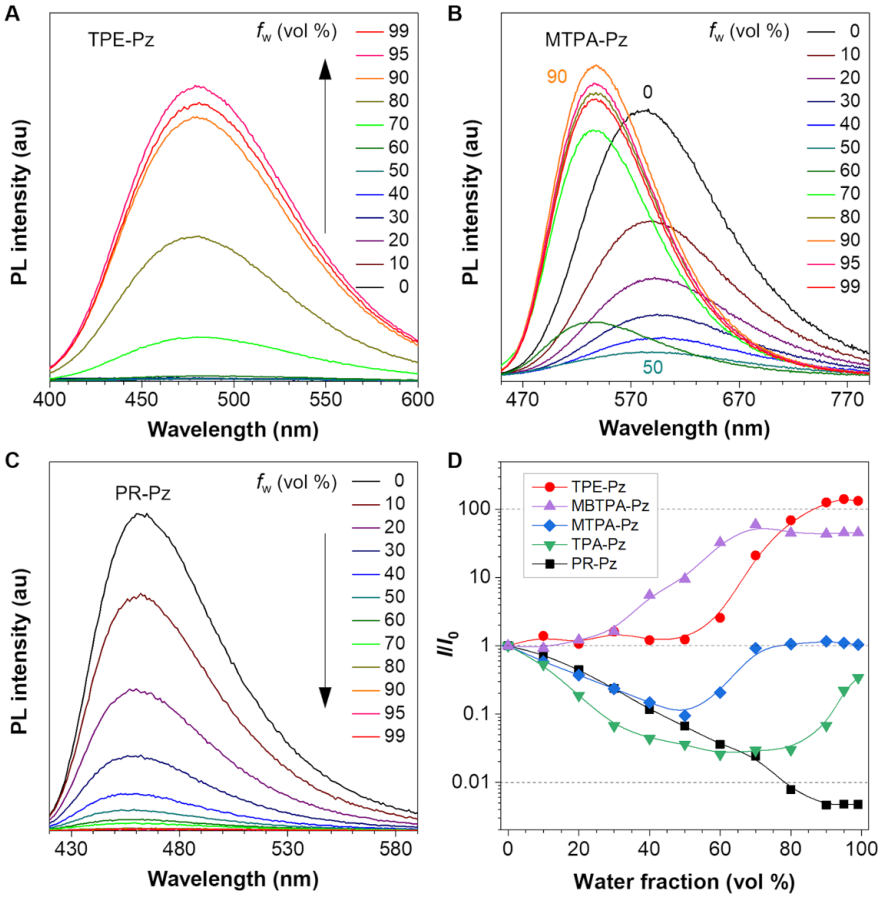

Figure 4. Aggregation-induced emissions of pyridazine adducts with AIEgens and aggregation-caused

quenching (ACQ) of a pyridazine adduct with an ACQ luminophore (ACQphore). PL spectra of (A) TPE-Pz, (B) MTPA-Pz, and (C) PR-Pz in the DMSO/water mixtures with different fractions of water (f_w). D) Plots of emission maxima of the pyridazine adducts with AIEgens or ACQphore against water fractions in the aqueous mixtures.

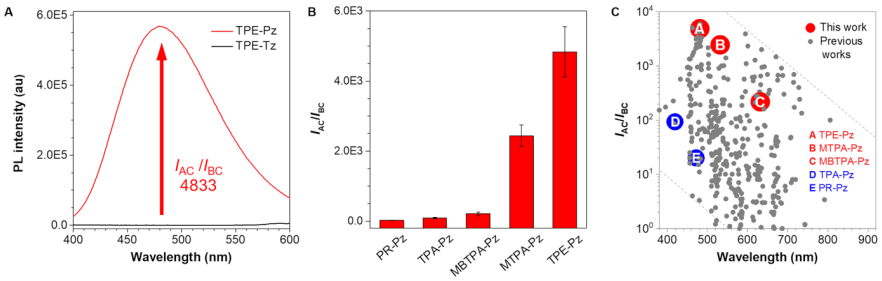

Figure 5. Emission enhancement upon iEDDA click reaction to AIEgen-tetrazine adducts in the aggregate state. A) PL spectra of TPE-Tz and TPE-Pz, with an enhancement ratio (I_{AC}/I_{BC}) of 4833, where I_{AC} and I_{BC} are the PL intensities after and before click reactions. B) Emission enhancement ratios of chromophore-tetrazine adducts by iEDDA click reaction in the aggregate state. C) Comparison of emission enhancement ratios between this and previous works.

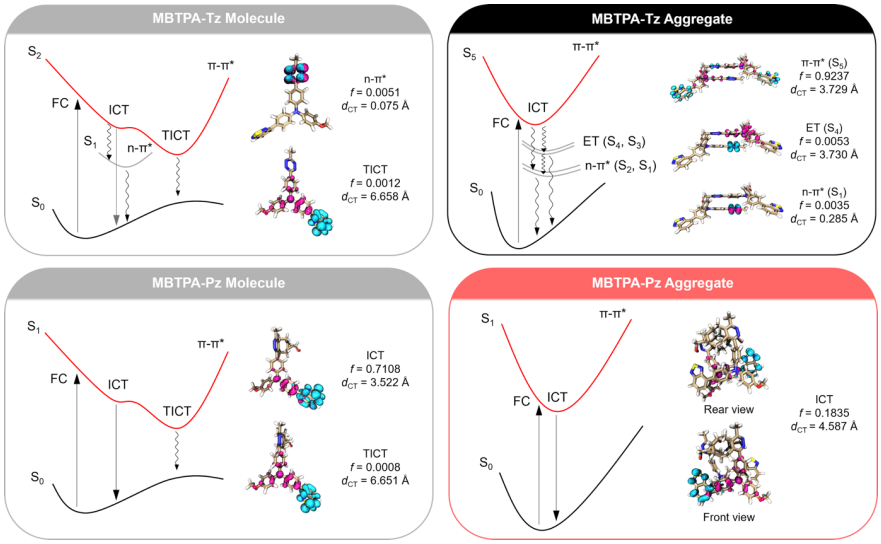

Figure 6. Schematic illustration of representative (de)excitation processes of tetrazine (Tz) and pyridazine (Pz) adducts of MBTPA at molecular and aggregate states, and hole/electron distributions obtained from quantum chemical calculations. The electron and hole are labeled in cyan and pink colors, respectively. FC = Franck–Condon state; ICT = intramolecular charge transfer state; TICT = twisted intramolecular charge transfer state; ET = electron transfer state; f = oscillator strength; d_{CT} = charge transfer distance.

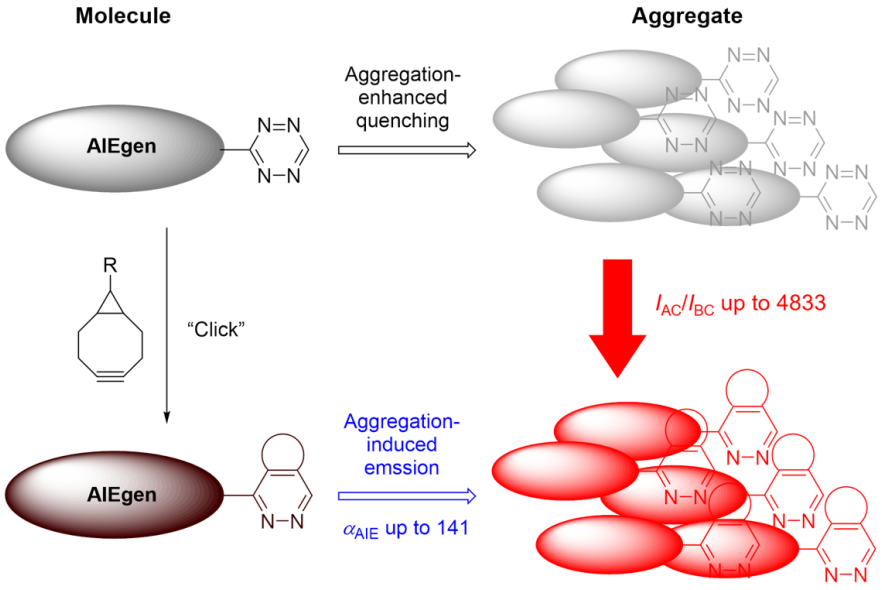

Figure 7. Proposed working mechanism for "Matthew Effect" in Aggregate Emission: upon aggregation, the "dark" AIEgen-Tz molecule becomes even darker, while the AIE-Pz molecule with the Tz moiety removed by the "click" reaction becomes more emissive, leading to the observed high emission enhancement ratio upon click reaction (I_{AC}/I_{BC} up to 4833).a_{AIE}: Emission enhancement ratio upon aggregation.

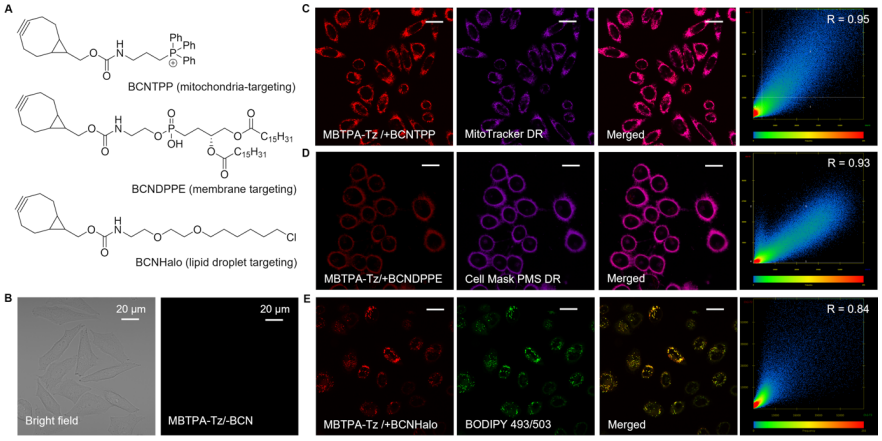

Figure 8. Confocal fluorescence imaging of living cells by the bioorthogonal reaction products of MBTPA-Tz with (A) BCN adducts carrying targeting units. B) Imaging of the living cells incubated in the presence of MBTPA-Tz without "click" with the BCN adducts. Fluorescence turned on by the *in situ* reactions of MBTPA-Tz with the BCN adducts carrying the targeting units specific to (C) mitochondria (red channel: λ_{ex} 405 nm, λ_{em} 600–700 nm; purple channel: λ_{ex} 640 nm, λ_{em} 600–700 nm), (D) cell membrane (red channel: λ_{ex} 405 nm, λ_{em} 550–700 nm; purple channel: λ_{ex} 561 nm, λ_{em} 550–700 nm), and (E) lipid droplet (red channel: λ_{ex} 405 nm, λ_{em} 495–602 nm; green channel: λ_{ex} 488 nm, λ_{em} 495–602 nm). R = Pearson correlation coefficient; DR = deep red; PMS = Plasma Membrane Stains. All scale bars are 20 μm.

Entry for the Table of Contents

"Matthew Effect" in Aggregate Emission: upon aggregation, dark species get darker and emissive species get brighter, resulting in significantly amplified turn-on emission upon bioorthogonal reaction.

Keywords : aggregation-induced emission, bioorthogonal chemistry, click chemistry, tetrazine, fluorescence imaging

Shinsuke Segawa, Xinwen Ou, Tianruo Shen, Tomohiro Ryu, Yuki Ishii, Herman H.Y. Sung, Ian D. Williams, Ryan T. K. Kwok, Ken Onda, Kiyoshi Miyata, Xuewen He, * Xiaogang Liu,*and Ben Zhong Tang*

Title "Matthew Effect": General Design Strategy of Fluorogenic Bioorthogonal Nanoprobes with Ultrahigh Emission Enhancement

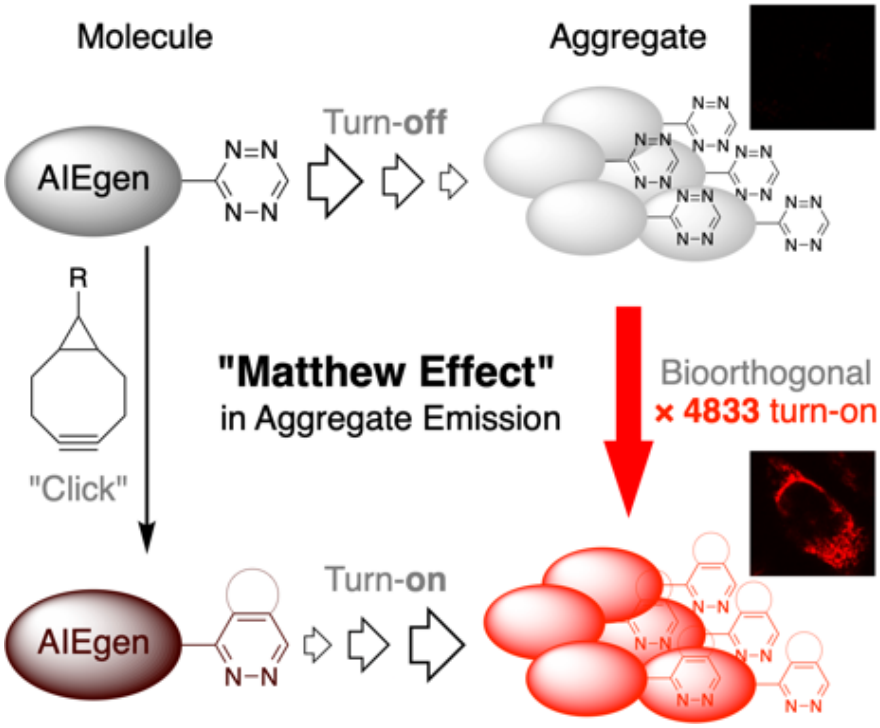

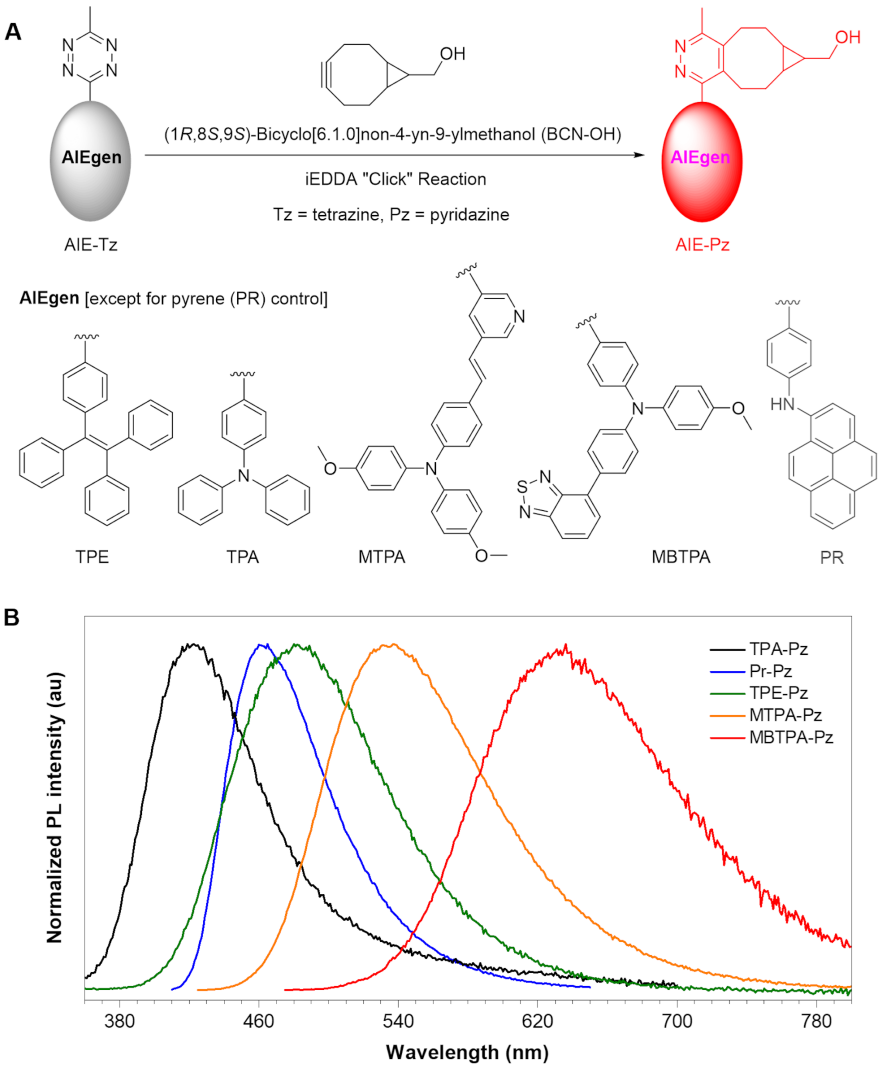

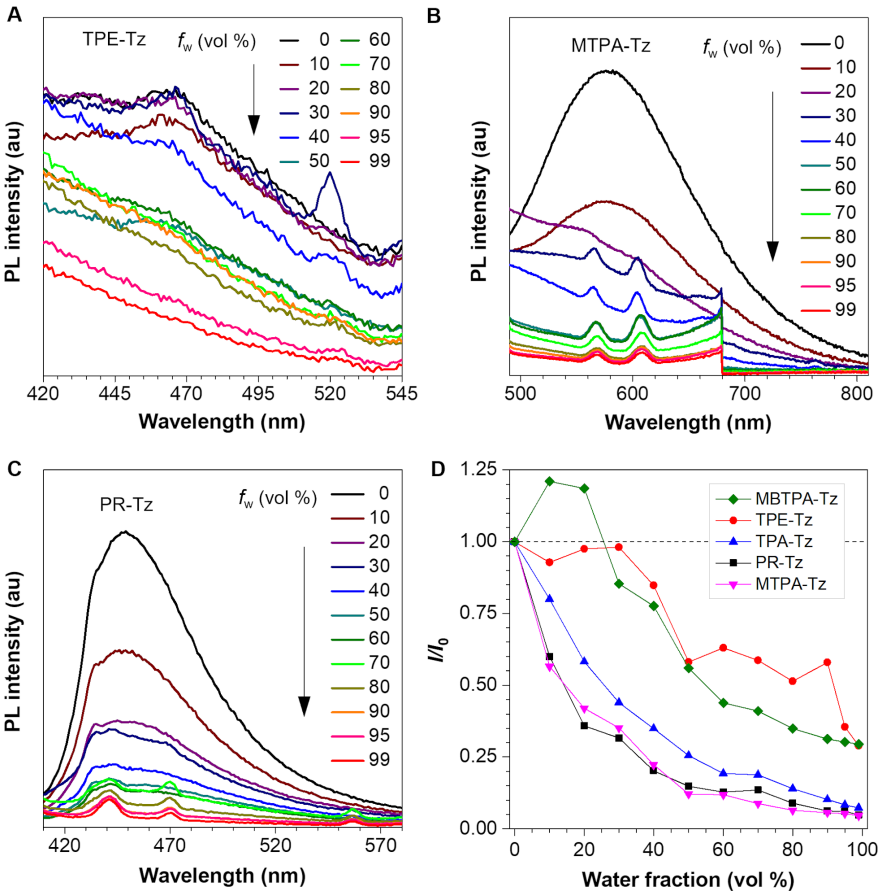

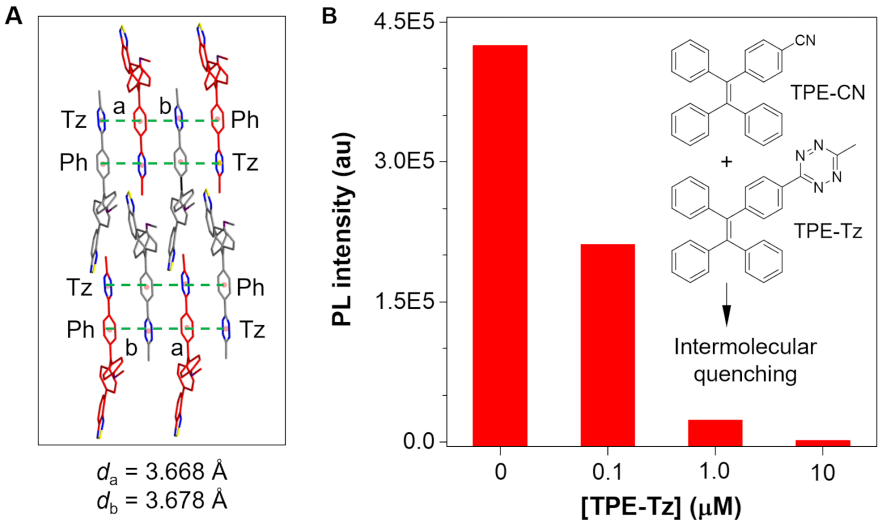

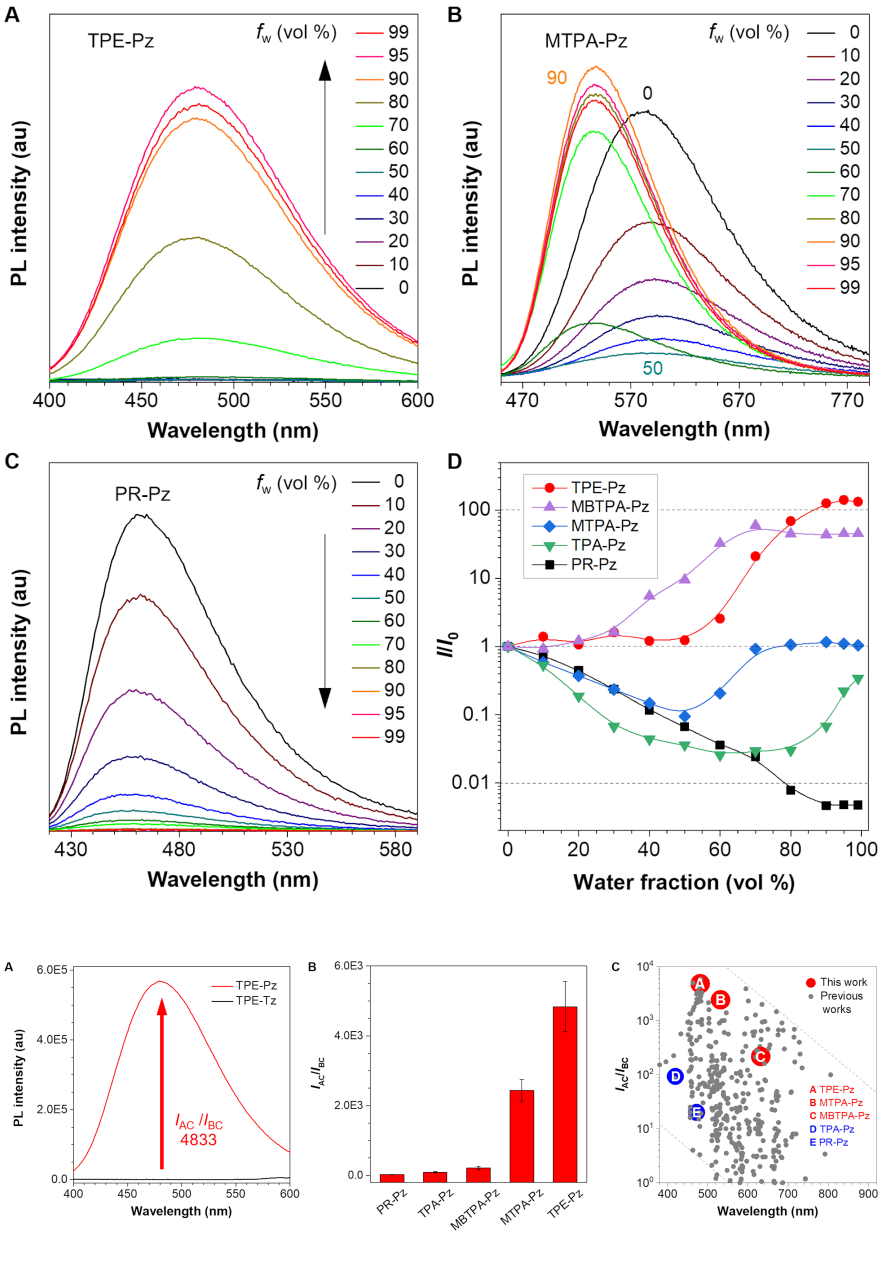

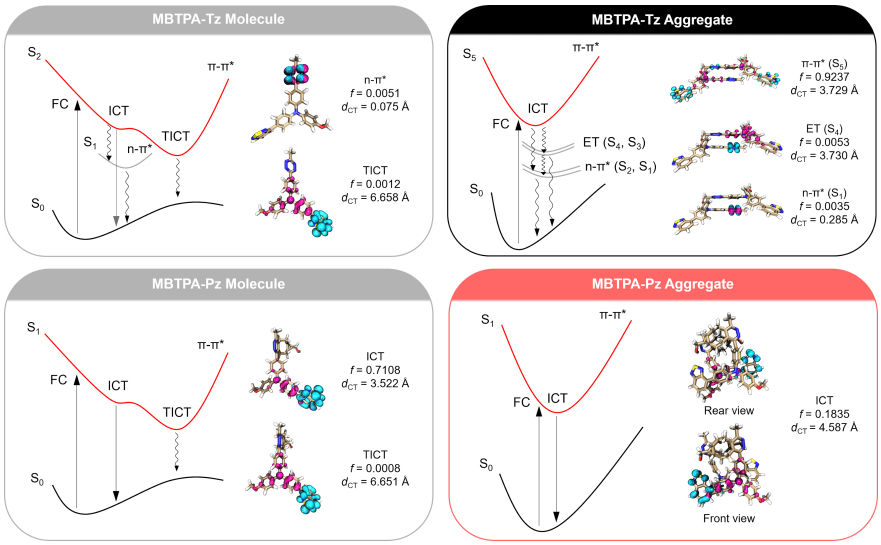

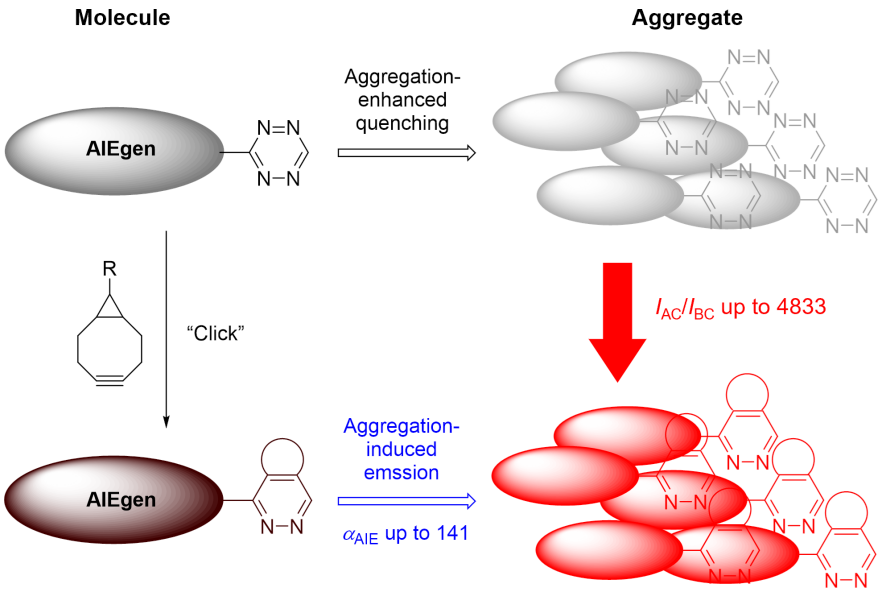

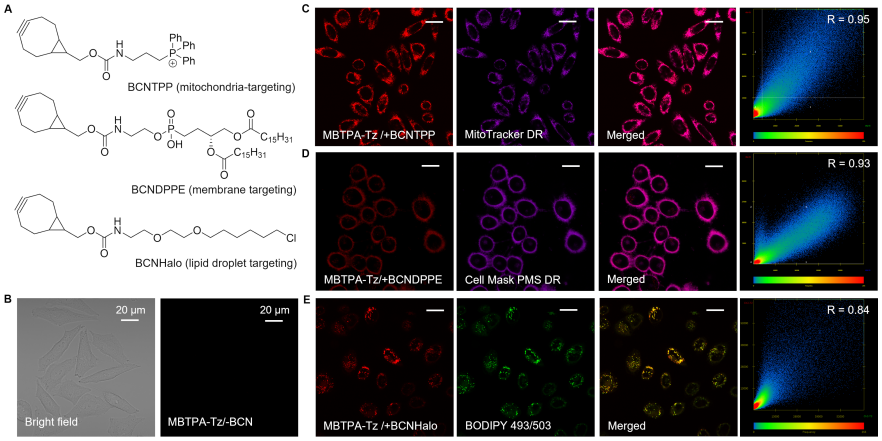

Aggregate Open Access WILEY

Title "Matthew Effect": General Design Strategy of Fluorogenic Bioorthogonal Nanoprobes with Ultrahigh Emission Enhancement

Shinsuke Segawa, Xinwen Ou, Tianruo Shen, Tomohiro Ryu, Yuki Ishii, Herman H.Y. Sung, Ian D. Williams, Ryan T. K. Kwok, Ken Onda, Kiyoshi Miyata, Xuewen He, * Xiaogang Liu,* and Ben Zhong Tang*

Shinsuke Segawa. Author 1.
Department of Chemical and Biological Engineering, School of Engineering
The Hong Kong University of Science and Technology
Kowloon, Hong Kong 999077, China

Dr. Xinwen Ou. Author 2, Dr. Herman H.Y. Sung. Author 6, Prof. Ian D. Williams. Author 7, Dr. Ryan T. K. Kwok. Author 8, Prof. Ben Zhong Tang. Author 13.
Department of Chemistry, Hong Kong Branch of Chinese National Engineering Research Center for Tissue Restoration and Reconstruction and Institute for Advanced Study
The Hong Kong University of Science and Technology
Kowloon, Hong Kong 999077, China
E-mail: tangbenz@cuhk.edu.cn

Tianruo Shen. Author 3, Prof. Xiaogang Liu. Author 12.
Science, Mathematics and Technology Cluster
Singapore University of Technology and Design
8 Somapah Road, 487372, Singapore
E-mail: xiaogang_liu@sutd.edu.sg

Tomohiro Ryu. Author 4, Yuki Ishii. Author 5, Prof. Ken Onda. Author 9, and Prof. Kiyoshi Miyata. Author 10.
Department of Chemistry, Graduate School of Science
Kyushu University
Motooka 744, Nishi-ku, Fukuoka 819-0395, Japan

Prof. Xuewen He, Author 11.
The Key Lab of Health Chemistry and Molecular Diagnosis of Suzhou, College of Chemistry, Chemical Engineering and Materials Science
Soochow University
199 Ren'ai Road, Suzhou, Jiangsu 215123, China
E-mail: xheao@suda.edu.cn

Prof. Ben Zhong Tang, Author 13.
School of Science and Engineering, Shenzhen Institute of Aggregate Science and Technology
The Chinese University of Hong Kong, Shenzhen
Guangdong 518172, China
E-mail: tangbenz@cuhk.edu.cn

Keywords: aggregation-induced emission, bioorthogonal chemistry, click chemistry, tetrazine, fluorescence imaging

Abstract:

Fluorescence imaging, a key technique in life science research, frequently utilizes fluorogenic probes for precise imaging in living systems. Tetrazine is an effective emission quencher in the design of fluorogenic probes, which can be selectively damaged upon bioorthogonal click reactions, leading to considerable emission enhancement. Despite significant efforts to increase the emission enhancement ratio upon click reaction (I_{AC}/I_{BC}) of tetrazine-functionalized fluorogenic probes, the influence of molecular aggregation on the emission properties has been largely overlooked in the design of these probes. In this study, we reveal that an ultrahigh I_{AC}/I_{BC} can be realized in the aggregate system when tetrazine is paired with aggregation-induced emission (AIE) luminogens. Tetrazine can increase its quenching efficiency upon aggregation and drastically reduce background emissions. Subsequent click reactions damage tetrazine and trigger significant AIE, leading to considerably enhanced I_{AC}/I_{BC}. We further showcase the capability of these ultra-fluorogenic systems in selective imaging of multiple organelles in living cells. We propose the term "Matthew Effect" in Aggregate Emission to describe the unique fluorogenicity of these probes, potentially providing a universal approach to attain ultrahigh emission enhancements in diverse fluorogenic aggregate systems.

1. Introduction

In recent decades, fluorescence imaging has emerged as a pivotal technique in life science for the direct visualization of dynamic living processes. Given the crowded nature of biological environments, achieving high-resolution imaging with an ultrahigh signal-to-noise ratio is of utmost importance for accurately monitoring chemical events. Therefore, significant efforts have been devoted to developing practical methodologies to obtain bright and high-resolution images. These strategies span from innovations in microscope design[1–6] and imaging system optimization[7] to intricate molecular-level[8–10] and nano-interface[11] engineering of fluorescent probes.

Fluorogenic probes, which refer to probes that can stimulate their emissions upon target recognition, represent a significant advancement in the pursuit of site-specific imaging with minimal background signals.[12,13] This milestone has been accomplished through the application of fluorescence quenching pathways.[14] For example, by linking an emission quencher to a fluorophore, the resulting fluorophore-quencher complex exhibits negligible emission. When the quencher is removed in response to specific biological events, the fluorophore's emission is restored, resulting in turn-on emission.[15] This characteristic defines the fluorophore-quencher complex as a fluorogenic probe. To enhance contrast and achieve site-specific signals with these fluorogenic probes, the identification of easily removable and highly effective emission quenchers is essential.

Tetrazine, a benzene-like molecule with four embedded nitrogen atoms, has been identified as an ideal moiety to possess the aforementioned tunable fluorescence quenching properties. The quenched emission can be fully recovered after the tetrazine quencher is controllably decomposed upon photoirradiation[16] or through inverse electron demand Diels-Alder (iEDDA) reaction with strained alkene[17–19], alkyne[20], or isonitrile[21,22] groups. The iEDDA reaction has been successfully employed as a bioorthogonal click reaction that can selectively and instantly occur in the molecularly crowded environment inside biological systems.[23] Consequently, tetrazine-based fluorogenic dyes have been extensively developed, with significant efforts aiming at enhancing their emission enhancement ratio (I_{AC}/I_{BC}, where I_{AC} and I_{BC} are the photoluminescence intensities after and before click reactions) by increasing tetrazine quenching efficiency. For example, initial studies started in the last decade focused on Förster Resonance Energy Transfer (FRET)[24,25] or through-bond energy transfer (TBET)[26,27] to direct n-π* emission quenching and ultrahigh I_{AC}/I_{BC} (>1000-fold) was achieved in blue to green probes via connecting fluorophore and tetrazine in proximity distance.[26] Later on, red to near-infrared turn-on emissions, which are challenging to attain through FRET or TBET-type quenching,[28] were realized by employing Dexter energy transfer (DET),[29] internal conversion

(IC),[30–33] and photo-induced electron transfer (PeT) directed by sophisticated control of molecular conformations.[34] As a unique approach, molecular disaggregation upon iEDDA reaction was also applied to enhance the I_{AC}/I_{BC} of near-infrared (NIR) cyanine dyes.[35] These tetrazine-based fluorogenic dyes have been successfully employed in bioorthogonal imaging of various cellular targets such as lipids,[36] sugars,[37] proteins,[38] and nucleic acids.[39] However, most previous molecules were developed as single molecular systems, neglecting the concentration quenching or aggregation-caused quenching (ACQ) effect in living cell systems: conventional hydrophobic fluorophores with large π-conjugated structures inherently assemble in aqueous solutions, turning off their emission and resulting in weak turn-on signals as fluorogenic probes.[40,41] Indeed, in many cases, I_{AC}/I_{BC} measurements were conducted in organic solvents where molecular aggregation can be prevented.[16,33,42–48] To achieve ultrahigh I_{AC}/I_{BC} in conditions that resemble cellular systems, it is desirable to develop fluorogenic systems in aggregate states.

Aggregation-induced emission luminogens (AIEgens) comprise a series of fluorescent dyes that exhibit weak emission in dilute solutions but can significantly enhance emission upon molecular aggregation.[49,50] Unlike conventional fluorophores that suffer from ACQ effects, AIEgens can achieve strong emissions even in aggregate states. Yet, there exist limited studies presenting tetrazine fluorogenic probes that exhibit aggregation-induced emission (AIE) properties post-iEDDA reaction.[51–53] One study reported a high I_{AC}/I_{BC} of up to 1779-fold, however it did not explicitly address the mechanism and relation between AIE properties and the high I_{AC}/I_{BC}.[51] Furthermore, the generalizability of such molecular design strategies remains unclear.

In this study, we demonstrated that by linking tetrazine to various AIEgens, the weakly-emissive tetrazine-AIEgen complex further suppresses their emission upon aggregation. Following an iEDDA reaction, the resulting emissive pyridazine compounds enhance their emission upon aggregation, affording ultrahigh I_{AC}/I_{BC}. Further investigation concludes that

this effect arises from the synergistic interplay between the intermolecular quenching effect of the tetrazine moiety and the AIE property of fluorogens. We also showcased that this ultra-fluorogenic system can be applied for site-selective fluorogenic imaging of multiple organelles in living cells, highlighting its potential for advanced imaging applications in biological systems. Drawing inspiration from the sociological term "Matthew Effect"[54] – describing the phenomenon that the rich become richer, and the poor become poorer – we coined this unique fluorogenisity as the "Matthew Effect" in Aggregate Emission, highlighting intensified darkness of quenched species and amplified brightness of emissive species in aggregate states. This "Matthew Effect" in Aggregate Emission potentially offers a universal strategy for achieving ultrahigh I_{AC}/I_{BC} in fluorogenic nanoaggregate systems.

2. Results and Discussion

2.1. Initial design and synthesis

To investigate how nano-aggregation and AIEgens will affect the turn-on emission of tetrazine probes, we designed and synthesized a series of tetrazine-dye conjugates. Tetrazine units were synthesized under Pinner synthesis using thiol as a catalyst,[55] and sequential Pd-catalyzed coupling reactions connected tetrazine to chromophores. The obtained compounds were recrystallized whenever it was possible, and purity was confirmed by high-performance liquid chromatography (HPLC) to avoid impurity effects (shown in Figure S81-S90, Supporting Information). Their molecular structures were thoroughly characterized by nuclear magnetic resonance (NMR) spectroscopy and high-resolution mass spectra (shown in Figures S25-S56, Supporting Information). Single crystals were obtained except for MTPA-Tz, and X-ray diffraction analysis supports the structure[56] (Figures S20-S23, in Supporting Information). We prepared four AIEgen-tetrazine conjugates (AIE-Tz) and one normal planar fluorophore:

pyrene-tetrazine conjugate (PR-Tz) as a negative control for the entire experiment. To obtain a multifaceted and general perspective of this strategy, we designed AIEgens with diverse structures that include either tetraphenyl ethylene (TPE-Tz) or triaryl amines (TPA-Tz, MTPA-Tz, and MBTPA-Tz) as well-known twisted units to achieve AIE properties. As expected, all molecules reacted quantitatively with the strained alkyne compound (1R,8S,9s)-Bicyclo[6.1.0]non-4-yn-9-ylmethanol (BCN-OH) to provide emissive pyridazine compounds (Figure 1A), and the obtained AIE-Pzs covered a broad emission range from violet to NIR (380 to 780 nm) in water (Figure 1B) with an emission maximum at 419 nm, 481 nm, 538 nm, 636 nm for TPA-Pz, TPE-Pz, MTPA-Pz, and MBTPA-Pz, respectively.

2.2. Photoluminescence measurements of AIE-Tz

After synthesizing AIE-Tz, we investigated their emission properties in dilute solutions in DMSO and aggregates in water. Not surprisingly, both AIE-Tzs and PR-Tz only exhibited very weak emissions in dilute solutions (quantum yield < 0.002, shown in Table S1, Supporting Information). This could be due to two reasons: firstly, AIEgens do not show strong emission in solution because of their molecular motions,[57] and secondly, the tetrazine unit acts as a quenching unit. However, we still observed non-negligible emissions from AIEgens or pyrene moieties that could cause background emission problems during fluorescence imaging. By changing the water fraction, molecular aggregation was observed with dynamic laser scattering measurements (Figure S5, Supporting Information). Interestingly, not only does PR-Tz, whose fluorophore is impacted by the aggregation-caused quenching effect, show further quenched emission upon molecular aggregation, but also AIE-Tzs, which are expected to exhibit enhanced emission, demonstrate further suppressed emission under the same conditions (Figure 2D), apart from the negligible emissions from the tetrazine moiety peaked at around 600 nm (Figure S2, Supporting Information). Specifically, TPE-Tz exhibited very weak emission at 470

nm coming from tetraphenyl ethylene core[58], and this emission's intensity decreased upon aggregation (Figure 2A). TPA-based tetrazine molecules displayed slightly stronger emission than TPE-Tz in dilute solution, and the emission was well quenched upon water addition (Figure 2B). This more notable emission of TPA tetrazine adducts over TPE-Tz could be a consequence of the less flexible structure of TPA units compared to TPE units. Indeed, PR-Tz, which has the most rigid structure, showed the strongest emission among all tetrazine compounds in DMSO, and a significant emission decrease was observed upon water addition (Figure 2C). This phenomenon of AIE-Tz suppressing its emission upon aggregation effectively highlights tetrazine's potential to reduce the background signals from fluorogenic dyes, thereby contributing to ultrahigh fluorescence turn-on ratios in the aggregate state. This intriguing observation further spurred our interest to explore this quenching effect more thoroughly.

2.3. Intermolecular quenching effect of AIE-Tz.

To understand why AIE-Tz exhibits emission quenching in the aggregate state despite the incorporation of AIEgens, we further investigated the interaction between the tetrazine moiety and AIEgens in the aggregate state. Single crystal X-ray diffraction (XRD) analysis and molecular dynamics (MD) simulations were conducted to obtain aggregate models of MBTPA-Tz, and intermolecular center-to-center distances between the tetrazine and surrounding aryl rings were calculated. As expected, we observed proximal molecular interactions in the aggregate state: 3.6-4.7 Å from the XRD result and 3.9-4.9 Å from the MD calculation (Figure S6-10, S24 in Supporting Information). The single crystal structure of MBTPA-Tz reveals a tetrazine-chromophore distance as close as 3.668 Å (Figure 3A). This distance is comparable to or even shorter than that of reported tetrazine fluorogenic dyes known to efficiently quench emissions through energy transfer mechanisms.[29] Therefore, this result indicates that tetrazine

can enhance emission quenching efficiency upon aggregation via intermolecular interactions with AIEgens. This intermolecular quenching effect of the tetrazine unit was experimentally confirmed using a commercially available AIEgen (TPE-CN) as a fluorescence indicator (Figure 3B). We measured the emission intensity of 10 μM TPE-CN, co-aggregated with TPE-Tz at different concentrations. Consequently, we observed that the emission of the aggregate was apparently quenched by 50.3% with 0.1 μM TPE-Tz addition; the emission intensity dropped 94.6% and even 99.7% with 1 μM and 10 μM TPE-Tz addition, respectively (Figure 3B). Considering there is no direct through-bond connection between TPE-CN and TPE-Tz, this quenching effect arises from intermolecular interactions between TPE-Tz and TPE-CN directed by aggregation.

2.4. Photoluminescence measurements of AIE-Pz

Tetrazine quenchers were easily converted to pyridazine moieties by BCN-OH addition, and the aggregate emission of the obtained AIE-Pz was next investigated. Similar to AIE-Tz, AIE-Pz forms aggregates upon increasing water fraction. Because the tetrazine quencher is removed, AIE-Pz exhibits stronger emission both in dilute solutions and aggregates (Table S1, Supporting Information). Most importantly, AIE-Pzs demonstrates enhanced emission upon aggregation, unlike AIE-Tzs (Figure 4D). Specifically, TPE-Pz and MBTPA-Pz display the most typical AIE properties (Figure 4A), with significantly increased emission upon water addition. In contrast, TPA-Pz and MTPA-Pz exhibit twisted-intramolecular charge transfer (TICT)[59] type AIEgen-like behavior: upon water addition, increased polarity causes charge separation in the excited state, initially quenching the emission. However, as the water fraction further increases, the emission is turned on again, induced by aggregate formation (Figure 4B). The PR-Pz negative control suffers from the ACQ effect and quenches its emission upon aggregation as

expected (Figure 4C). In short, we achieved an emission enhancement system in AIE-Pzs aggregates.

2.5. Turn-on emissions of AIE-Tz upon "click" reaction

We successfully achieved a unique system in which non-emissive tetrazine molecules become even darker, and emissive pyridazine molecules become even brighter in aggregate states. Encouraged by this result, we calculated the emission enhancement ratio upon click reaction (I_{AC}/I_{BC}) in the aggregate state to verify the impact of this aggregation-formation strategy on the emission enhancement ratio. The PR-Tz negative control demonstrated a very weak I_{AC}/I_{BC} around 20 in an aqueous environment due to the strong ACQ effect in water (Figure 5B) In contrast, TPE-Tz, possessing the most canonical AIEgen unit, displayed a significantly high emission enhancement ratio of I_{AC}/I_{BC} up to 4833 (Figure 5A, C). Even TPA derivatives, which act as less active AIE units, resulted in a high emission enhancement ratio upon click reaction (Figure S4, Supporting Information), as evidenced by MTPA-Tz (I_{AC}/I_{BC} = 2439) and MBTPA-Tz (I_{AC}/I_{BC} = 209). Only TPA-Tz did not exhibit strong turn-on emission (I_{AC}/I_{BC} = 93) among AIE-Tz, as the post-click reaction compound was still affected by n-π* type quenching from the pyridazine group and did not exhibit a strong emission (quantum yield < 0.02, Table S1 and Figure S16 in Supporting Information).

Multiple reports suggest a negative correlation between emission wavelengths[25,28,60] and emission enhancement ratios for tetrazine fluorogenic probes. To confirm this, we plotted I_{AC}/I_{BC} values of previously reported tetrazine dyes against their emission wavelength. As a result, the plotted data points revealed a distinct and consistent trend, illustrating that as the emission wavelength increased, the emission enhancement ratio decreased. This visualization successfully substantiated the negative correlation between these two parameters. Most importantly, we observed that AIE-Tz demonstrated a very strong turn-on property compared

to previously reported molecules in each emission wavelength. Notably, the 4833-fold emission enhancement of TPE-Tz is one of the best values among previous reports (Figure 5C and Table S2, Supporting Information). In conclusion, we discovered that connecting AIEgens to tetrazine units is an effective and general strategy for achieving strong fluorogenic signals in aqueous systems that inevitably cause aggregation of hydrophobic molecules.

2.6. Theoretical investigation of tetrazine quenching mechanism

To better understand the quenching mechanism and turn-on mechanism, density functional theory (DFT) and time-dependent DFT (TD-DFT) calculations were carried out on MBTPA-Tz and its post-iEDDA reaction compound MBTPA-Pz in single molecule and aggregate states. We focused on these molecules considering MBTPA-Pz's long emission wavelength and high $I_{AC}/I_{BC,}$ which is ideal for biological applications. A comprehensive explanation of the assignment process for individual excited states can be found in section 3 of Supporting Information.

Tetrazine moieties cause significant emission quenching through various mechanisms. In general, the primary quenching mechanism involves accessing the dark n-π* transition state in the tetrazine moiety. When the tetrazine moiety is conjugated with a chromophore, this access comes from the internal conversion process, termed internal conversion to dark state (ICDS).[31] Alternatively, when access comes from energy transfer processes such as FRET[60] or DET[29] between tetrazine and fluorophore, the quenching process is summarized as energy transfer to dark state (ETDS).[25] Additionally, when tetrazine is located close to a fluorophore, the electron-deficient tetrazine unit can act as a strong acceptor, causing a non-radiative electron-transferred (ET) state through the PeT mechanism.[34] At the same time, AIEgens with highly twisted and rotational structures are well known to quench their emission through molecular motion.[57] As one of the molecular flexibility triggering quenching states, we focused on the

twisted-intramolecular charge transfer (TICT)[59,61] state, in which molecules are twisted to intramolecularly separate charge between electron-rich and electron-poor moieties that cause weaker emission.

When we investigate our system (Figure 6), not surprisingly, we observed two major non-radiative states under the emissive π-π* state in MBTPA-Tz molecular state: 1) the dark n-π* state caused by the tetrazine unit and 2) the TICT state caused by the AIEgen. Those states were confirmed as dark states by their negligible oscillator strength values ($f < 0.01$). For MBTPA-Tz, tetrazine is conjugated with AIEgen; therefore, the access to the dark n-π* state is from internal conversion. We determined that emission quenching is due to both ICDS and TICT processes. Once MBTPA-Tz is aggregated, the dark state characteristics change. Restricted molecular configuration prohibits access to the TICT quenching state. Instead, we found a newly formed dark ET state whose hole and electron are separated in two molecules, accompanied by low-lying dark n-π* states induced by the tetrazine moieties.

This result matches the intermolecular quenching effect observed in AIE-Tz molecules: close interaction between tetrazine and AIEgen induces PeT quenching and provides intermolecular access to the n-π* dark state through energy transfer as well as maintaining internal conversion pathways. In summary, MBTPA-Tz aggregate quenches emission based on ICDS, ETDS, and PeT processes. These multiple quenching pathways amplify the quenching effect of tetrazine and explain the experimental result of the aggregation-enhanced quenching effect of MBTPA-Tz (Figure 2).

Upon iEDDA reaction, the tetrazine moiety is damaged, and the tetrazine-triggered quenching states are henceforward eliminated. As a result, the pyridazine molecule exhibits different behavior. In the single-molecule state of MBTPA-Pz, the n-π* dark state is no longer observed, but the twisted-intramolecular charge transfer (TICT) state persists, resulting in weak fluorescence in dilute solution. However, when aggregation occurs, the TICT formation is restricted due to the limited free volume and hydrophobic environment in the solid state.

Consequently, no quenching state exists beneath the emissive π-π* state, allowing for strong emission in the MBTPA-Pz aggregate. As a result, the emission of MBTPA-Pz is switched on as access to the TICT dark state is inhibited in the aggregate state.

2.7. "Matthew Effect" in Aggregate Emission

In short, we successfully developed a system in which non-emissive tetrazine-containing molecules become even less emissive, and emissive pyridazine molecules become even more emissive in the aggregate state, resulting in ultra-high emission enhancement ratios. We refer to this effect as the "Matthew Effect" in Aggregate Emission (Figure 7), drawing from the sociological term that describes the phenomenon in which the poor become poorer, and the rich become richer in academic society.[54] Given that the intermolecular quenching effect is not limited to the tetrazine moiety, we anticipate additional "Matthew Effect" in Aggregate Emission reports in the future, which can be designed by connecting AIEgens to emission quencher.

2.8. Bioorthogonal fluorogenic live cell imaging

Lastly, we applied the fluorogenic nanoaggregate for bioorthogonal fluorogenic imaging in living cells. First, MBTPA-Tz was added to cells, and confocal laser microscopy was used to observe the emission signals inside the cells. As expected, no emission was observed even after a 60 min incubation (Figure 8B). After washing the cells thoroughly, BCN-OH was added and incubated for 30 min, resulting in the observation of turn-on emission inside the cell without the washing procedure (Figure S18, Supporting Information). This result confirms that the iEDDA reaction between MBTPA-Tz and BCN-OH can bioorthogonaly take place in congested living systems.

To utilize this bioorthogonal turn-on emission for more specific purposes, the hydroxy group of BCN-OH was functionalized with several side chains targeting specific organelles: a triphenylphosphine group (TPP) to target mitochondria, a 1,2-dipalmitoyl-sn-glycero-3-phosphoethanolamine (DPPE) unit to target the cell membrane, and a halotag ligand (Halo) to localize to the hydrophobic environment inside the cell. These compounds were designated as BCNTPP, BCNDPPE, and BCNHalo, correspondingly (Figure 8A). The biocompatibility of MBTPA-Tz and these BCN compounds were confirmed by MTT assay (Figure S17). By adding BCNTPP or BCNHalo to cells incubated with MBTPA-Tz, strong turn-on emission was observed at the mitochondria and lipid droplets, respectively. Here, excellent colocalization signals alongside commercially available organelle-staining dyes (MitoTracker™ Deep Red FM and BODIPY™ 493/503) were observed, with Pearson correlation coefficients up to 0.95 and 0.84 (Figure 8C, E), respectively. However, when BCNDPPE was added, no turn-on emission was observed at the cell membrane. This could likely be attributed to BCNDPPE being initially internalized into the cell and taking some time to be expressed on the cell surface. To address this problem, BCNDPPE was added first and allowed to incubate for 24 hours, followed by a thorough washing of the cells and the subsequent addition of MBTPA-Tz. As a result, strong turn-on emission was observed at the cellular membrane (Figure 8D), which was further confirmed by colocalized signals using a commercially available membrane tracker (CellMask™ Plasma Membrane Stains) with a Pearson correlation coefficient of up to 0.93. Consequently, MBTPA-Tz aggregates were proven to selectively target and visualize biological targets labeled with a strained alkyne group. To our best knowledge, this is the first example of tetrazine functionalized AIEgen for imaging multiple cellular environments. Previous reports only addressed to mitochondria imaging applications.[51–53] Therefore, this result highlights the flexible localization property of AIEgen-based nanoprobe, which expands the applications of this bioorthogonally activatable fluorogenic systems. Furthermore, it is noteworthy that it shows better photo-bleaching stability than any commercially available bioprobes used in this

study (Figure S19, Supporting Information). These compelling findings provide substantial evidence that the MBTPA-Tz nanoprobe can effectively serve as a versatile biological imaging tool, as demonstrated by its exceptional multi-organelle targeting capabilities.

3. Conclusion

In this study, we have demonstrated a general strategy to develop ultra-highly fluorogenic tetrazine probes: By connecting a tetrazine quencher to an AIEgen, we observed a unique feature where non-emissive tetrazine compounds further quench their emission upon aggregation, and emissive pyridazine compounds enhance their emission upon aggregation. We termed this effect, which significantly enhances the emission enhancement ratio, as the "Matthew Effect" in Aggregate Emission.

Based on the experimental and theoretical investigation, we concluded that this "Matthew Effect" in Aggregate Emission arises from the synergetic effects of intermolecular quenching of the tetrazine moiety and aggregation-induced emission properties induced by AIEgens.

Lastly, we demonstrated that this highly fluorogenic aggregate can be applied for bioorthogonal fluorogenic imaging in living cells: by controlling the BCN location, we can observe turn-on signals in specific cellular environments such as mitochondria, cellular membranes, and lipid droplets. Considering recent advances in bioorthogonal chemistry to non-genetically label biological systems with clickable handles, this fluorogenic aggregate will become a key tool to visualize various molecular events inside living systems.

Based on its mechanism, the "Matthew Effect" in Aggregate Emission is expected to be realized not only by tetrazine but also by any emission quenchers when they are connected to an AIEgen. Therefore, this report will pave the way for a general strategy to achieve high turn-on emissions by transcending single molecular properties through aggregate formation.

Acknowledgements

We would like to express our deepest gratitude to Prof. Terence Wong at The Hong Kong University of Science and Technology, Prof. Motonari Uesugi at Kyoto University, Dr. Hiromichi V. Miyagishi at Hokkaido University, Prof. Neal K. Devaraj at the University of California, San Diego, and Prof. K. Barry Sharpless and Dr. John Cappiello at Scripps Research for their invaluable guidance, comments, and insightful suggestions. The authors acknowledge the funding support of Hong Kong PhD Fellowship Scheme (PF18-15484), the National Natural Science Foundation of China (21788102 and 22274106), the Research Grants Council of Hong Kong (16306620, 16303221, N_HKUST609/19, and C6014-20W), the Innovation and Technology Commission (ITC-CNERC14SC01), and Shenzhen Science and Technology Innovation Committee (JCYJ20180507183832744). This work was partly supported by JSPS KAKENHI (JP23H01977, JP23H04631), JST the establishment of university fellowships towards the creation of science technology innovation (JPMJFS2132).

Conflict of Interests

The authors declare no conflict of interests.

Data Availability Statement

The data that supports the findings of this study are available in the supplementary material of this article

Supporting Information

Supporting Information is available from the Wiley Online Library or from the author.

Aggregate Open Access

WILEY

Received: ((will be filled in by the editorial staff))
Revised: ((will be filled in by the editorial staff))
Published online: ((will be filled in by the editorial staff))

References

[1] M. G. L. Gustafsson, *Proc. Natl. Acad. Sci. U. S. A.* **2005**, *102*, 13081.

[2] E. Betzig, G. H. Patterson, R. Sougrat, O. W. Lindwasser, S. Olenych, J. S. Bonifacino, M. W. Davidson, J. Lippincott-Schwartz, H. F. Hess, *Science* **2006**, *313*, 1642.

[3] S. T. Hess, T. P. K. Girirajan, M. D. Mason, *Biophys. J.* **2006**, *91*, 4258.

[4] M. J. Rust, M. Bates, X. Zhuang, *Nat. Methods* **2006**, *3*, 793.

[5] S. W. Hell, J. Wichmann, *Opt. Lett.* **1994**, *19*, 780.

[6] Z. Liu, L. D. Lavis, E. Betzig, *Mol. Cell* **2015**, *58*, 644.

[7] A. Sharonov, R. M. Hochstrasser, *Proc. Natl. Acad. Sci. U. S. A.* **2006**, *103*, 18911.

[8] S.-N. Uno, M. Kamiya, T. Yoshihara, K. Sugawara, K. Okabe, M. C. Tarhan, H. Fujita, T. Funatsu, Y. Okada, S. Tobita, Y. Urano, *Nat. Chem.* **2014**, *6*, 681.

[9] J. Tyson, K. Hu, S. Zheng, P. Kidd, N. Dadina, L. Chu, D. Toomre, J. Bewersdorf, A. Schepartz, *ACS Cent Sci* **2021**, *7*, 1419.

[10] Q. Zheng, A. X. Ayala, I. Chung, A. V. Weigel, A. Ranjan, N. Falco, J. B. Grimm, A. N. Tkachuk, C. Wu, J. Lippincott-Schwartz, R. H. Singer, L. D. Lavis, *ACS Cent Sci* **2019**, *5*, 1602.

[11] X. Yang, K. Zhanghao, H. Wang, Y. Liu, F. Wang, X. Zhang, K. Shi, J. Gao, D. Jin, P. Xi, *ACS Photonics* **2016**, *3*, 1611.

[12] X. Li, X. Gao, W. Shi, H. Ma, *Chem. Rev.* **2014**, *114*, 590.

[13] G. A. Lemieux, C. L. De Graffenried, C. R. Bertozzi, *J. Am. Chem. Soc.* **2003**, *125*, 4708.

[14] M. J. Hangauer, C. R. Bertozzi, *Angew. Chem. Int. Ed* **2008**, *47*, 2394.

[15] S. Leng, Q.-L. Qiao, Y. Gao, L. Miao, W.-G. Deng, Z.-C. Xu, *Chin. Chem. Lett.* **2017**, *28*, 1911.

[16] A. Loredo, J. Tang, L. Wang, K.-L. Wu, Z. Peng, H. Xiao, *Chem. Sci.* **2020**, *11*, 4410.

[17] N. K. Devaraj, R. Weissleder, S. A. Hilderbrand, *Bioconjug. Chem.* **2008**, *19*, 2297.

[18] D. M. Patterson, L. A. Nazarova, B. Xie, D. N. Kamber, J. A. Prescher, *J. Am. Chem. Soc.* **2012**, *134*, 18638.

[19] M. L. Blackman, M. Royzen, J. M. Fox, *J. Am. Chem. Soc.* **2008**, *130*, 13518.

[20] K. Lang, L. Davis, S. Wallace, M. Mahesh, D. J. Cox, M. L. Blackman, J. M. Fox, J. W. Chin, *J. Am. Chem. Soc.* **2012**, *134*, 10317.

[21] J. Tu, D. Svatunek, S. Parvez, A. C. Liu, B. J. Levandowski, H. J. Eckvahl, R. T. Peterson, K. N. Houk, R. M. Franzini, *Angew. Chem. Int. Ed.* **2019**, *58*, 9043.

[22] M. Xu, T. Deb, J. Tu, R. M. Franzini, *J. Org. Chem.* **2019**, *84*, 15520.

[23] C. P. Ramil, Q. Lin, *Chem. Commun.* **2013**, *49*, 11007.

[24] N. K. Devaraj, S. Hilderbrand, R. Upadhyay, R. Mazitschek, R. Weissleder, *Angew. Chem. Int. Ed.* **2010**, *49*, 2869.

[25] W. Chi, L. Huang, C. Wang, D. Tan, Z. Xu, X. Liu, *Mater. Chem. Front* **2021**, *5*, 7012.

[26] L. G. Meimetis, J. C. T. Carlson, R. J. Giedt, R. H. Kohler, R. Weissleder, *Angew. Chem. Int. Ed.* **2014**, *53*, 7531.

[27] G. Knorr, E. Kozma, A. Herner, E. A. Lemke, P. Kele, *Chem Eur J* **2016**, *22*, 8972.

[28] L. Chen, F. Li, M. Nandi, L. Huang, Z. Chen, J. Wei, W. Chi, X. Liu, J. Yang, *Dyes Pigm.* **2020**, *177*, 108313.

[29] P. Werther, K. Yserentant, F. Braun, K. Grußmayer, V. Navikas, M. Yu, Z. Zhang, M. J. Ziegler, C. Mayer, A. J. Gralak, M. Busch, W. Chi, F. Rominger, A. Radenovic, X. Liu, E. A. Lemke, T. Buckup, D.-P. Herten, R. Wombacher, *ACS. Cent. Sci.* **2021**, *7*, 1561.

[30] Y. Lee, W. Cho, J. Sung, E. Kim, S. B. Park, *J. Am. Chem. Soc.* **2018**, *140*, 974.

[31] T. Shen, W. Zhang, P. Yadav, X. W. Sun, X. Liu, *Mater. Chem. Front.* **2023**, *7*, 1082.

[32] T. S.-M. Tang, H.-W. Liu, K. K.-W. Lo, *Chem. Commun.* **2017**, *53*, 3299.

[33] W. Mao, J. Tang, L. Dai, X. He, J. Li, L. Cai, P. Liao, R. Jiang, J. Zhou, H. Wu, *Angew. Chem. Int. Ed.* **2021**, *60*, 2393.

[34] W. Mao, W. Chi, X. He, C. Wang, X. Wang, H. Yang, X. Liu, H. Wu, *Angew. Chem. Int. Ed.* **2022**, *61*, e202117386.

[35] X. Zhang, J. Gao, Y. Tang, J. Yu, S. S. Liew, C. Qiao, Y. Cao, G. Liu, H. Fan, Y. Xia, J. Tian, K. Pu, Z. Wang, *Nat. Commun.* **2022**, *13*, 3513.

[36] L. Chen, F. Li, Y. Li, J. Yang, Y. Li, B. He, *Chem. Commun.* **2021**, *58*, 298.

[37] S. Stairs, A. A. Neves, H. Stöckmann, Y. A. Wainman, H. Ireland-Zecchini, K. M. Brindle, F. J. Leeper, *Chembiochem* **2013**, *14*, 1063.

[38] J. L. Seitchik, J. C. Peeler, M. T. Taylor, M. L. Blackman, T. W. Rhoads, R. B. Cooley, C. Refakis, J. M. Fox, R. A. Mehl, *J. Am. Chem. Soc.* **2012**, *134*, 2898.

[39] P. N. Asare-Okai, E. Agustin, D. Fabris, M. Royzen, *Chem. Commun.* **2014**, *50*, 7844.

[40] G. S. Beddard, S. E. Carlin, G. Porter, *Chem. Phys. Lett.* **1976**, *43*, 27.

[41] Y. Huang, J. Xing, Q. Gong, L.-C. Chen, G. Liu, C. Yao, Z. Wang, H.-L. Zhang, Z. Chen, Q. Zhang, *Nat. Commun.* **2019**, *10*, 169.

[42] W. Shi, J. Li, X. He, S. Zhou, H. Sun, H. Wu, *Org. Lett.* **2022**, *24*, 3368.

[43] P. E. Z. Klier, A. M. M. Gest, J. G. Martin, R. Roo, M. X. Navarro, L. Lesiak, P. E. Deal, N. Dadina, J. Tyson, A. Schepartz, E. W. Miller, *J. Am. Chem. Soc.* **2022**, *144*, 12138.

[44] M. E. Graziotto, L. D. Adair, A. Kaur, P. Vérité, S. R. Ball, M. Sunde, D. Jacquemin, E. J. New, *RSC Chem Biol* **2021**, *2*, 1491.

[45] S. J. Siegl, J. Galeta, R. Dzijak, M. Dračínský, M. Vrabel, *Chempluschem* **2019**, *84*, 493.

[46] D. Wu, D. F. O'Shea, *Chem. Commun.* **2017**, *53*, 10804.

[47] A. Yazdani, N. Janzen, S. Czorny, R. G. Ungard, T. Miladinovic, G. Singh, J. F. Valliant, *Dalton Trans.* **2017**, *46*, 14691.

[48] H. Wu, J. Yang, J. Šečkutė, N. K. Devaraj, *Angew. Chem. Int. Ed* **2014**, *53*, 5805.

[49] J. Luo, Z. Xie, J. W. Y. Lam, L. Cheng, H. Chen, C. Qiu, H. S. Kwok, X. Zhan, Y. Liu, D. Zhu, Others, *Chem. Commun.* **2001**, 1740.

[50] Y. Hong, J. W. Y. Lam, B. Z. Tang, *Chem. Soc. Rev.* **2011**, *40*, 5361.

[51] Y. Wang, Y. Teng, H. Yang, X. Li, D. Yin, Y. Tian, *Chem. Commun.* **2022**, *58*, 949.

[52] S.-K. Choi, Y. Lee, S. E. Yoon, H. Choi, J. Kim, J. H. Kim, S. Lee, W. Kim, E. Kim, *Sens. Actuators B Chem.* **2021**, *340*, 129966.

[53] Y. Teng, R. Zhang, B. Yang, H. Yang, X. Li, D. Yin, X. Feng, Y. Tian, *J. Mater. Chem. B.* **2022**, *10*, 8642.

[54] R. K. Merton, *Science* **1968**, *159*, 56.

[55] W. Mao, W. Shi, J. Li, D. Su, X. Wang, L. Zhang, L. Pan, X. Wu, H. Wu, *Angew. Chem. Int. Ed.* **2019**, *58*, 1106.

[56] CCDC 2263531 (for PR-Tz), 2263532 (for MBTPA-Tz), 2263533 (for TPA-Tz), and 2263534 (for TPE-Tz) contain the supplementary crystallographic data for this paper. These data can be obtained free of charge from The Cambridge Crystallographic Data Centre via www.ccdc.cam.ac.uk/structurese.

[57] N. L. C. Leung, N. Xie, W. Yuan, Y. Liu, Q. Wu, Q. Peng, Q. Miao, J. W. Y. Lam, B. Z. Tang, *Chem. Eur. J.* **2014**, *20*, 15349.

[58] L. Huang, H. Tao, S. Zhao, K. Yang, Q.-Y. Cao, M. Lan, *Ind. Eng. Chem. Res.* **2020**, *59*, 8252.

[59] S. Sasaki, G. P. C. Drummen, G.-I. Konishi, *J. Mater. Chem.* **2016**, *4*, 2731.

[60] B. Pinto-Pacheco, W. P. Carbery, S. Khan, D. B. Turner, D. Buccella, *Angew. Chem. Int. Ed* **2020**, *59*, 22140.

[61] K. Hanaoka, S. Iwaki, K. Yagi, T. Myochin, T. Ikeno, H. Ohno, E. Sasaki, T. Komatsu, T. Ueno, M. Uchigashima, T. Mikuni, K. Tainaka, S. Tahara, S. Takeuchi, T. Tahara, M. Uchiyama, T. Nagano, Y. Urano, *J. Am. Chem. Soc.* **2022**, *144*, 19778.

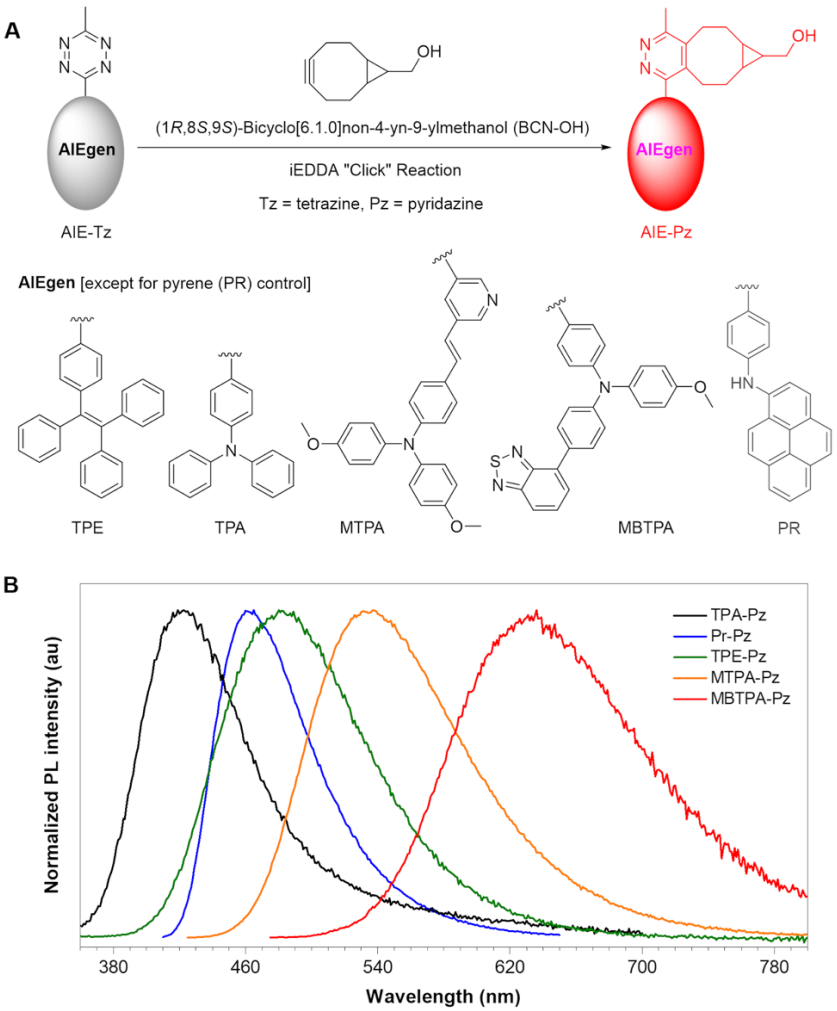

Figure 1. A) Design of fluorogenic probe using tetrazine (Tz) as an emission quencher and BCN-OH as a turn-on switch; AIE = aggregation-induced emission, AIEgen = AIE luminogen, iEDDA = inverse electron-demand Diels-Alder. B) Photoluminescence (PL) spectra of the fluorogens synthesized in this work.

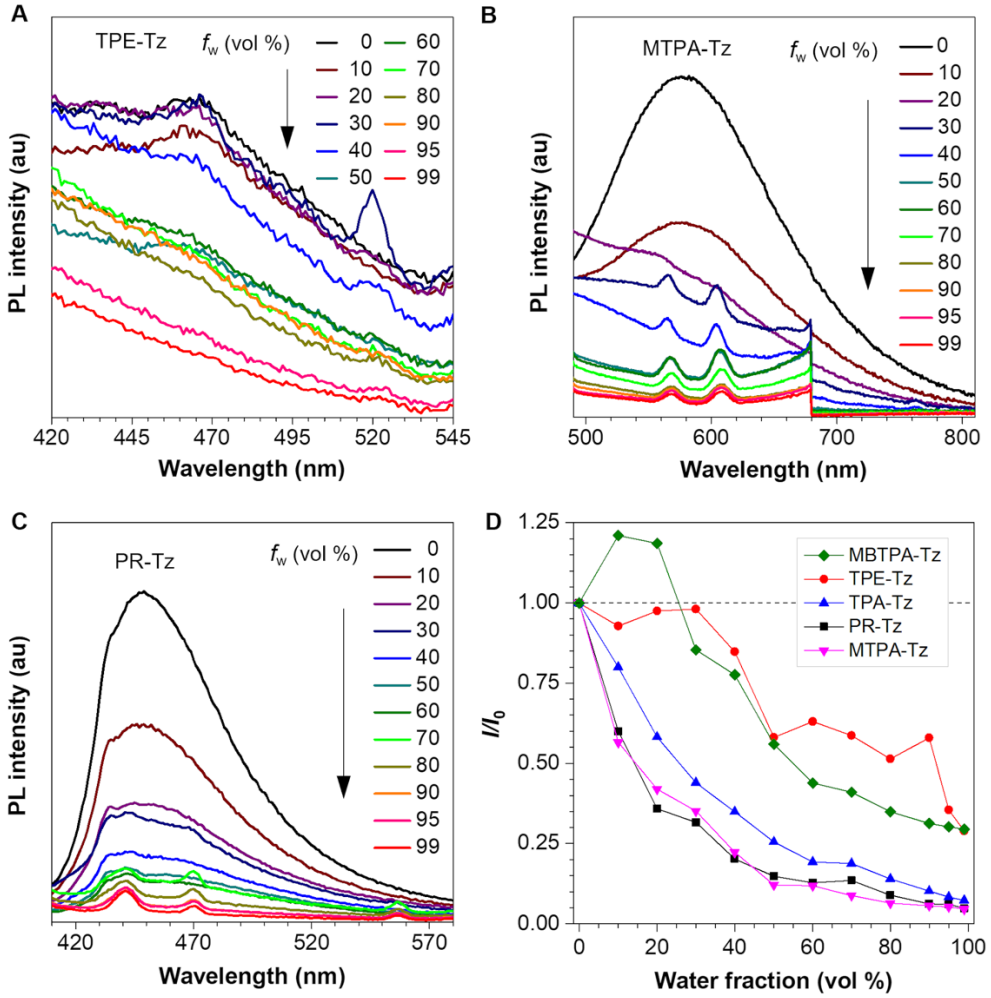

Figure 2. Aggregation-enhanced quenching of chromophore-tetrazine (Ch-Tz) adducts. PL spectra of (A) TPE-Tz, (B) MTPA-Tz, and (C) PR-Tz in the DMSO/water mixtures with different fractions of water (f_w). D) Plots of emission maxima of Ch-Tz adducts against water fractions in the aqueous mixtures. It needs to be noted that since the compounds are all dark tetrazine species, the emission intensities here are significantly low. Therefore, some inevitable noise was also captured to obtain these minimum signals with this magnified view. Nevertheless, most importantly, a clear trend of enhanced quenching upon aggregation was observed.

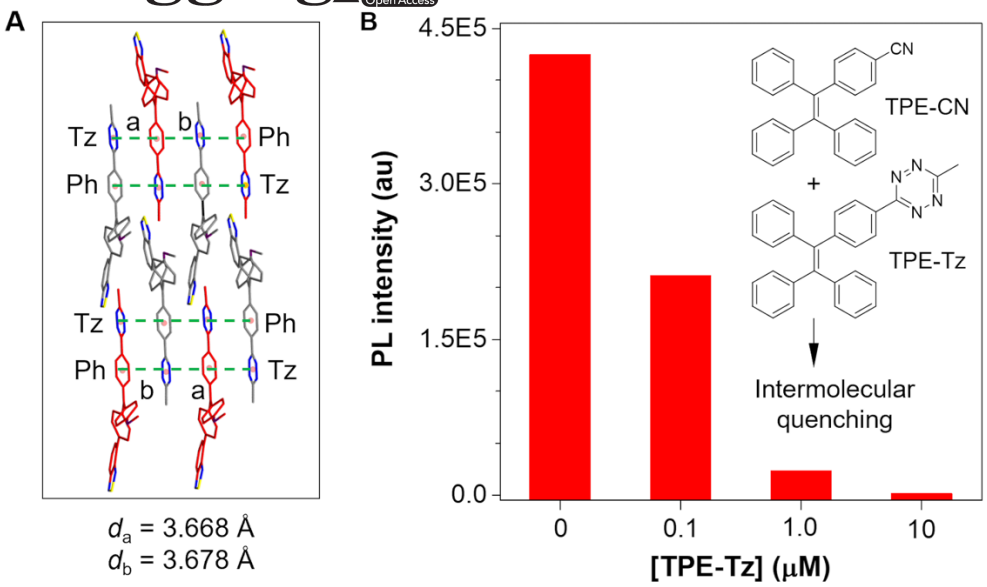

Figure 3. A) Intermolecular interaction between tetrazine (Tz; acceptor) and phenyl (Ph; donor) rings in the crystal structure of MBTPA-Tz. B) PL quenching of TPE-CN (10 μM) by the intermolecular interaction with TPE-Tz in their aggregates in the DMSO/water mixture (f_w = 99 vol %). *d* = distance.

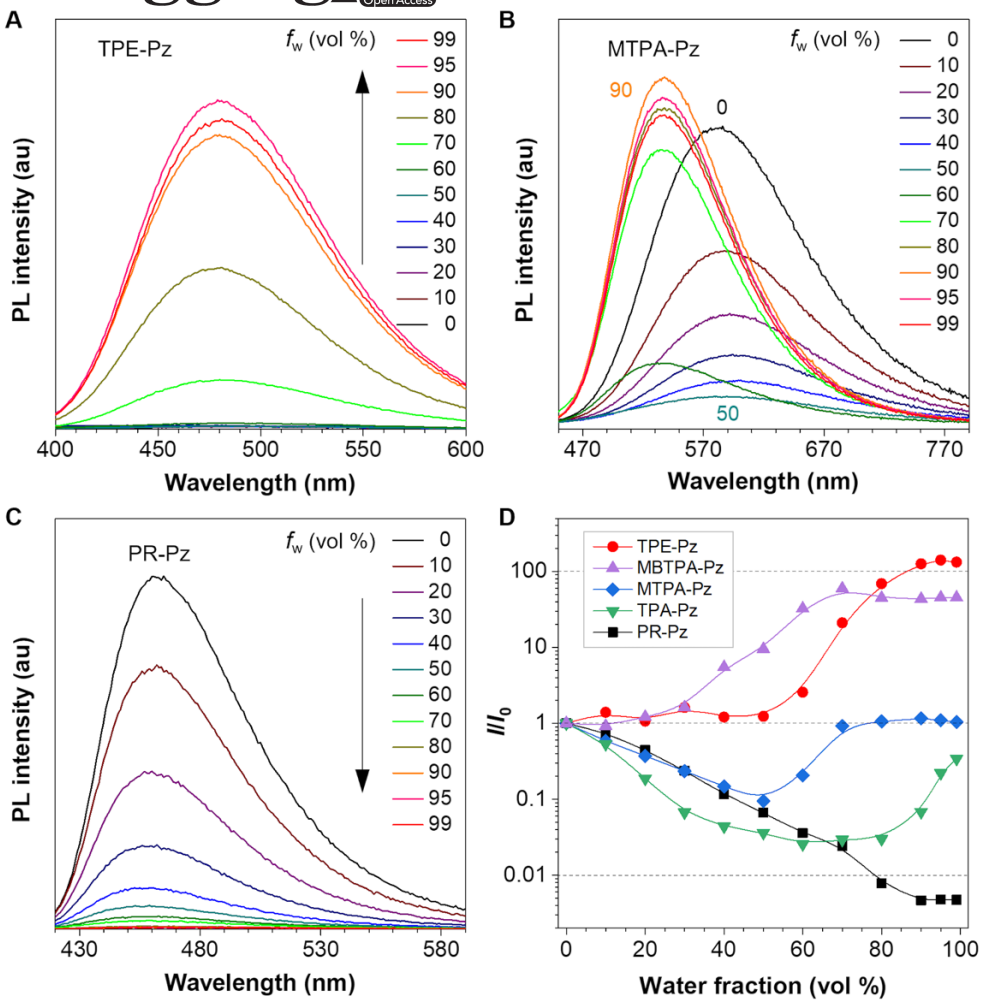

Figure 4. Aggregation-induced emissions of pyridazine adducts with AIEgens and aggregation-caused quenching (ACQ) of a pyridazine adduct with an ACQ luminophore (ACQphore). PL spectra of (A) TPE-Pz, (B) MTPA-Pz, and (C) PR-Pz in the DMSO/water mixtures with different fractions of water (f_w). D) Plots of emission maxima of the pyridazine adducts with AIEgens or ACQphore against water fractions in the aqueous mixtures.

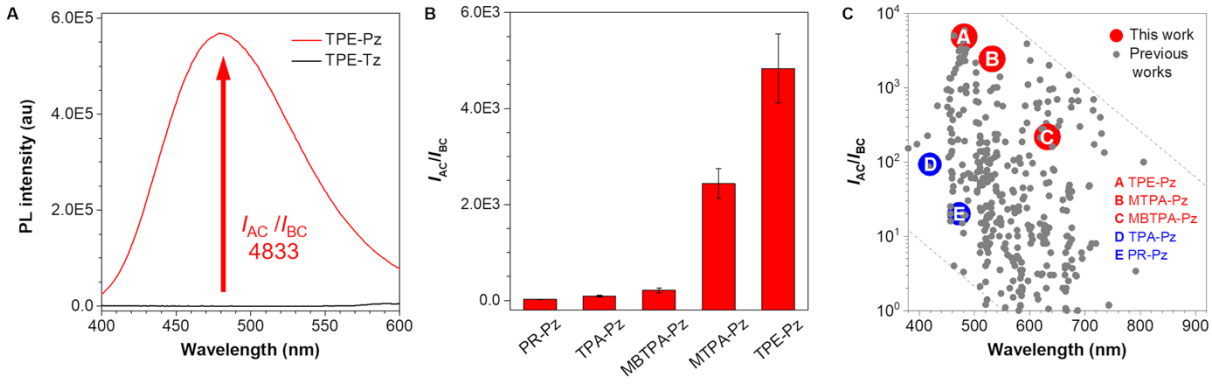

Figure 5. Emission enhancement upon iEDDA click reaction to AIEgen-tetrazine adducts in the aggregate state. A) PL spectra of TPE-Tz and TPE-Pz, with an enhancement ratio (I_{AC}/I_{BC}) of 4833, where I_{AC} and I_{BC} are the PL intensities after and before click reactions. B) Emission enhancement ratios of chromophore-tetrazine adducts by iEDDA click reaction in the aggregate state. C) Comparison of emission enhancement ratios between this and previous works.

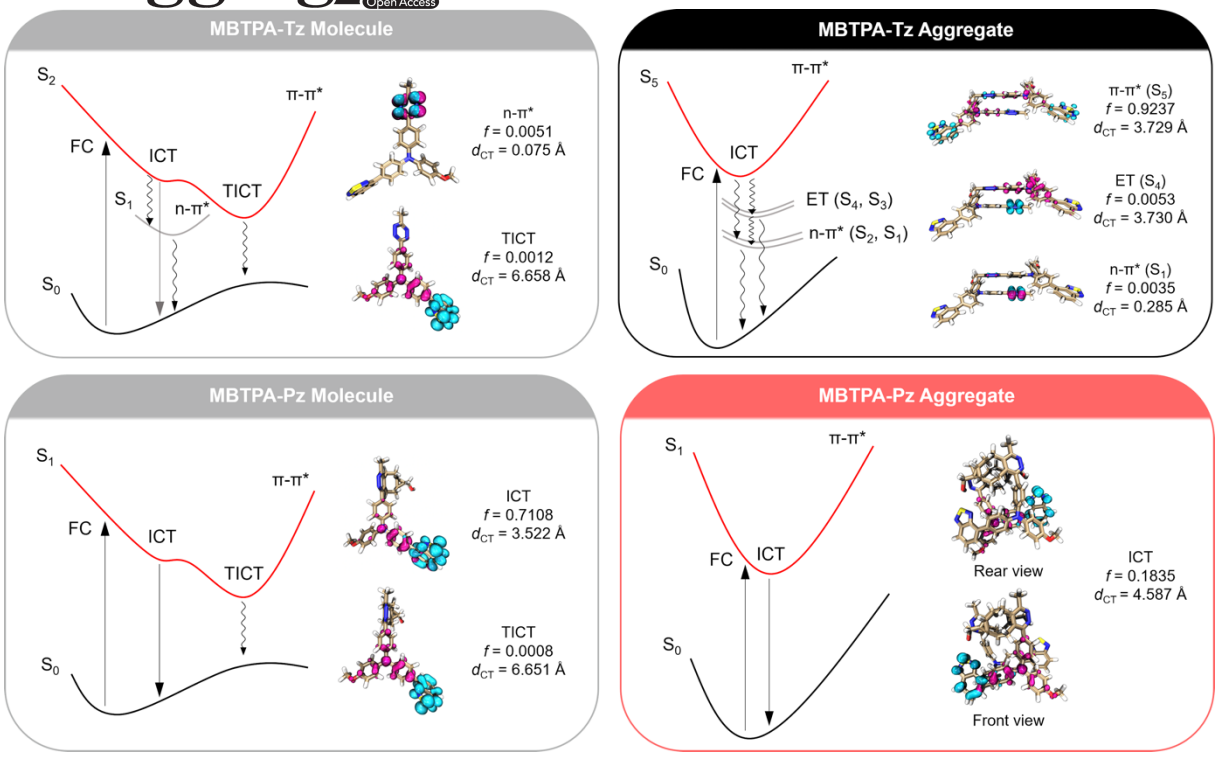

Figure 6. Schematic illustration of representative (de)excitation processes of tetrazine (Tz) and pyridazine (Pz) adducts of MBTPA at molecular and aggregate states, and hole/electron distributions obtained from quantum chemical calculations. The electron and hole are labeled in cyan and pink colors, respectively. FC = Franck–Condon state; ICT = intramolecular charge transfer state; TICT = twisted intramolecular charge transfer state; ET = electron transfer state; f = oscillator strength; d_{CT} = charge transfer distance.

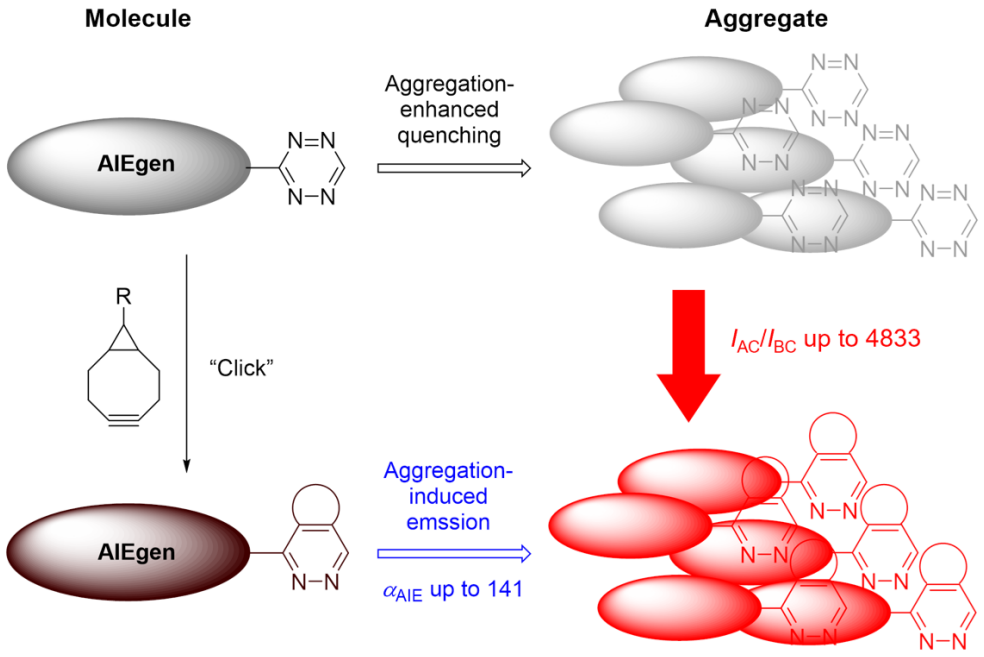

Figure 7. Proposed working mechanism for "Matthew Effect" in Aggregate Emission: upon aggregation, the "dark" AIEgen-Tz molecule becomes even darker, while the AIE-Pz molecule with the Tz moiety removed by the "click" reaction becomes more emissive, leading to the observed high emission enhancement ratio upon click reaction (I_{AC}/I_{BC} up to 4833). α_{AIE}: Emission enhancement ratio upon aggregation.

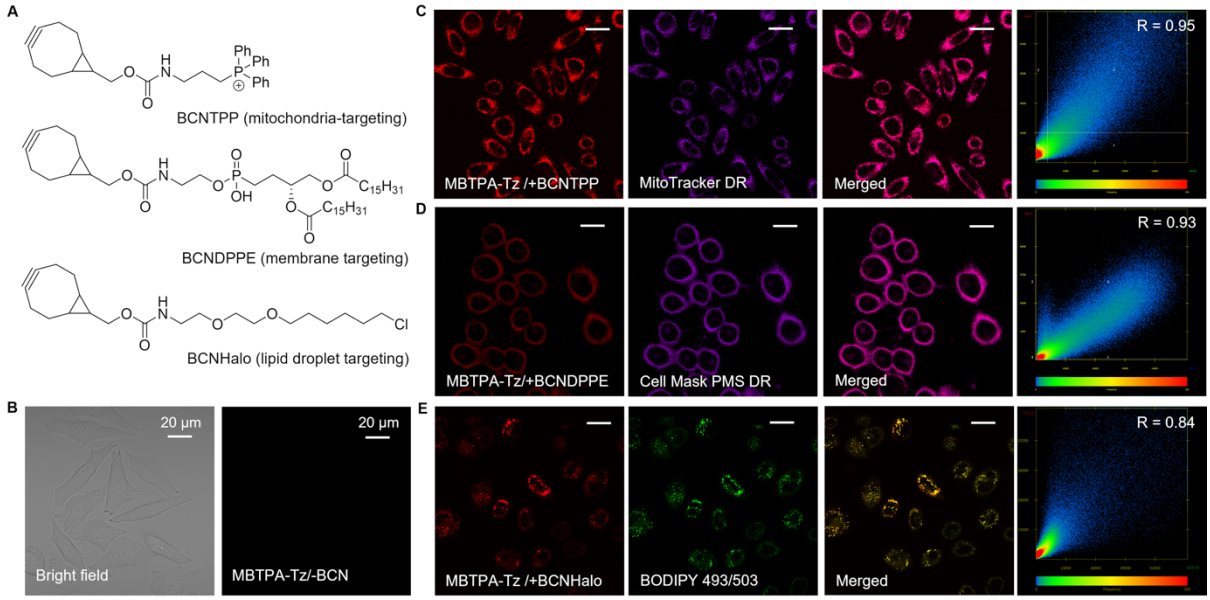

Figure 8. Confocal fluorescence imaging of living cells by the bioorthogonal reaction products of MBTPA-Tz with (A) BCN adducts carrying targeting units. B) Imaging of the living cells incubated in the presence of MBTPA-Tz without "click" with the BCN adducts. Fluorescence turned on by the *in situ* reactions of MBTPA-Tz with the BCN adducts carrying the targeting units specific to (C) mitochondria (red channel: λ_{ex} 405 nm, λ_{em} 600–700 nm; purple channel: λ_{ex} 640 nm, λ_{em} 600–700 nm), (D) cell membrane (red channel: λ_{ex} 405 nm, λ_{em} 550–700 nm; purple channel: λ_{ex} 561 nm, λ_{em} 550–700 nm), and (E) lipid droplet (red channel: λ_{ex} 405 nm, λ_{em} 495–602 nm; green channel: λ_{ex} 488 nm, λ_{em} 495–602 nm). R = Pearson correlation coefficient; DR = deep red; PMS = Plasma Membrane Stains. All scale bars are 20 μm.

Aggregate Open Access WILEY

Entry for the Table of Contents

"Matthew Effect" in Aggregate Emission: upon aggregation, dark species get darker and emissive species get brighter, resulting in significantly amplified turn-on emission upon bioorthogonal reaction.

Keywords: aggregation-induced emission, bioorthogonal chemistry, click chemistry, tetrazine, fluorescence imaging

Shinsuke Segawa, Xinwen Ou, Tianruo Shen, Tomohiro Ryu, Yuki Ishii, Herman H.Y. Sung, Ian D. Williams, Ryan T. K. Kwok, Ken Onda, Kiyoshi Miyata, Xuewen He, * Xiaogang Liu,* and Ben Zhong Tang*

Title "Matthew Effect": General Design Strategy of Fluorogenic Bioorthogonal Nanoprobes with Ultrahigh Emission Enhancement